A parametric optimisation study of urban geometry design to assess outdoor thermal comfort.

Yasser Ibrahim[a], Tristan Kershaw[a,*], Paul Shepherd[a] and Ibrahim Elwy[b]

[a]Department of Architecture and Civil Engineering, University of Bath, Bath BA2 7AY, UK.

[b]Department of Architecture Engineering, Military Technical College, Cairo 11662, Egypt.

y.m.m.ibrahim@bath.ac.uk, t.j.kershaw@bath.ac.uk, p.shepherd@bath.ac.uk, Ibrahim.elwy@live.com

[*]Correspondence: t.j.kershaw@bath.ac.uk, +44(0)1225 384984

Abstract

Over the last two decades, urban geometry has been shown to be a key determinant of the microclimatic conditions in urban areas. This study uses the Ladybug-tools, the plugins of Grasshopper3D to optimise building heights, street widths and orientation to maximise outdoor thermal comfort, represented by the diurnal average Universal Thermal Climate Index (UTCI). In the hot-arid climate of Cairo, Egypt, the optimised parameters of symmetrical and asymmetrical urban canyons are compared with the Egyptian Construction Act's design regulations. The results show a strong negative correlation between the height-to-width (H/W) ratios and the output UTCI, with $R^2 = 0.71$, and much stronger ($R^2 = 0.91$) if east-west orientations are excluded from the results, exceeding correlations previously reported for Cairo. Maximum UTCI reductions due to changing H/W and orientation approach ~6 °C. Considerable variation is shown in the strength of the correlation between UTCI and the asymmetrical H/W ratio of each flank, with $R^2 = 0.81$ for Southeast side compared to $R^2 = 0.4$ for Northwest side. Design recommendations are given urban planners based on using the optimised parameters that at least achieve a UTCI reduction benchmark that exceeds those resulting from using the regulations' thresholds.

Keywords: Thermal comfort, UTCI, Urban geometry, Ladybug, Optimisation

1 Introduction

Urban areas are expected to accommodate almost 70% of the global population by 2050 (United Nations, 2018). With such global urbanisation rates, increasing attention has been paid to the negative environmental impacts of urban areas, and many discussions on the resilience and liveability of current

and future urban developments have expanded to include other environmental qualities such as urban health and well-being. The impact of the urban microclimate on public health has already been documented (Kovats *et al.*, 2008), and over the past three decades, the attention given to outdoor thermal comfort as one of the key performance indicators for urban environmental assessment has grown (Jamei *et al.*, 2016). For outdoor urban environments, thermal comfort is temporal and is dependent on the inter-connectivity of the physiological and micro-climatological conditions (Coccolo *et al.*, 2016), where pedestrians are exposed to large fluctuations in air temperatures, wind velocities and solar irradiation over time. Moreover, the thermal stress-induced sensation can drive pedestrians into adaptation practices, i.e. increasing dependency on automobiles and use of indoor space, which in turn increases their associated energy consumption and greenhouse gas emissions (Futcher *et al.*, 2013). Given knowledge of human thermoregulation and the recent development of computational models (Naboni *et al.*, 2019a), comfort metrics have become easier to understand and more viable to quantify. Indeed, the integration of these metrics in climate-responsive design policies and guidelines has become an inevitable practice (Ruefenacht *et al.*, 2020), although this is not fully realised across the globe.

Densification of the built environment leads to the replacement of permeable surfaces with impervious construction materials, reduced vegetation, increased pollution, and relatively narrower canyon ratios. Dubbed the urban heat island (UHI), Oke (1995) articulated the negative impacts that urban areas pose to the microclimate. This includes increased long-wave radiation absorption as a result of air pollution and the sensible heat storage due to the higher thermal admittance of building constructions. Evaporative cooling is also limited by impervious paving and reduced percolation, while anthropogenic heat is released into the local environment from buildings and traffic. Canyon geometry is another crucial factor, with recurrent reflections trapping short-wave radiation at street level, leading to greater absorption and attenuating net long-wave radiation loss, as well as inhibiting turbulent heat transfer by convection (Oke, 1995; Toparlar *et al.*, 2015). In this context, urban form plays a crucial role in shaping the microclimatic conditions to which pedestrians are exposed, and hence the perceived thermal comfort. Studies that have investigated canyon geometry in temperate and humid climates are abundant (Qaid *et al.*, 2015; Sharmin *et al.*, 2017), as opposed to those conducted in hot and dry areas,

though the latter accommodates about one-third of the world's population (Pearlmutter *et al.*, 2007). Given the interdependencies of the energy budgets of urban elements, in-situ measurements are typically laborious compared to computational simulations. In this regard, there has been significant interest among bio-climatologists to develop computational models capable of estimating human thermal comfort in response to their ever-changing surrounding thermal environment (Naboni *et al.*, 2017). Additionally, the tendency to engage parametric design tools within urban environmental simulations has increased remarkably, where the exploration of a myriad of design solutions is feasible (Wagdy *et al.*, 2017).

1.1 Urban geometry

The planetary boundary layer, the lowest layer of the Earth's atmosphere, is partitioned into an urban canopy layer (UCL) which extends from the street level up to the mean height of the roughness elements, i.e. buildings and trees, and the urban boundary layer (UBL) which can extend to up to 2km above the city (Ampatzidis *et al.*, 2020). Besides the thermal mixing and level of moisture and pollutant content of the atmosphere, the height, spacing and configuration of the urban roughness elements dictate the air flow characteristics, and hence shape the structure and the depth of the UBL (Oke *et al.*, 2017). At a city scale, neighbourhoods with similar land use and land cover can generate different local microclimates due to several factors, among which are urban morphology, construction materials, provision of vegetation and human activity (Stewart *et al.*, 2012). Urban forms comprise of several urban canyons with varying geometric parameters such as canyon orientation, street width (W), building heights (H), canyon aspect ratio (H/W), and sky view factors (Ali-Toudert *et al.*, 2006). These different configurations, together with other surface-specific parameters, e.g. albedo and emissivity (Andreou, 2013), and environmental parameters, e.g. air temperatures, humidity, wind speed and solar irradiation, are sufficient to modulate the radiant exchanges and wind flow patterns within the canyon, resulting in distinct microclimatic conditions for an urban canyon (Grimmond *et al.*, 2010). The local climate of given urban form could be implied from the microclimatic performance of these canyons (Fahmy, 2010; Lin *et al.*, 2017). Hot-dry areas are accompanied by substantial heat stress, due to the increased magnitude of short-wave solar radiation and increased long-wave radiation emitted from urban surfaces,

and hence should not accommodate dispersed urban forms typical of hot-humid areas (Ratti *et al.*, 2003). However, the suitability of a given urban layout for a specific climate remains a function of the geometrical proportions, which might if changed significantly, entail a radical change in performance (Golany, 1996).

The influence of canyon aspect ratio on the microclimate is disparate, with its induced thermal performance being highly dependent on the climatic region. A higher H/W ratio (lower sky view factor) reduces the amount of solar radiation received and absorbed by the urban surfaces, entailing lower daytime temperatures, albeit with slightly higher nocturnal temperatures (Johansson, 2006), partially due to trapping the long-wave radiation within the street canyon (known as the canyon effect). As a result, abundant studies have acknowledged that higher H/W ratios can be beneficial in dry climates (Ahmed, 1994; Bourbia *et al.*, 2010), while others have argued their benefits due to lower wind penetration and reduced cooling rates (Giannopoulou *et al.*, 2010; Niachou *et al.*, 2008). In terms of their shading effect, studies conducted in various climatic regions have attested that improved thermal comfort levels can be achieved by the shading generated by increased building heights (Ali-Toudert *et al.*, 2007; Perini *et al.*, 2014). On the other hand, studies investigating canyon orientation in different climates have shown significant variability. Street orientation, unless notably wide, defines the diurnal course of the canyon's solar exposure. However, seasonal variations play as important a role as the orientation. Thus, an "optimum" orientation is ostensibly unattainable, and a "preferred" one should be a trade-off between hot and cold seasons. Nonetheless, East-West (E-W) canyons have been reported to maintain the worst daily thermal conditions, particularly during summer, owing to increased solar exposure (Watkins *et al.*, 2007). In this sense, North-South (N-S), NE-SW, and NW-SE oriented canyons have been advocated by many studies to be appropriate within arid, semi-arid, and Mediterranean climates (Jamei *et al.*, 2019), while others have claimed the suitability of E-W canyons for temperate and Mediterranean climates only if galleries and overhanging facades are used (Ali-Toudert, 2005). Furthermore, a canyon's airflow is influenced by its geometry (H/W ratio and the orientation) and is governed by the mean wind at the average roof level. In simple terms, the lower the H/W ratio, the less undisturbed airflow there is above the canopy layer. H/W ratios of ~0.05 are

characterised by an isolated roughness flow. This is disturbed by the canyon's flow as the H/W increases up to 0.7 and is turned into a wake interference flow with deflection-reinforced eddies generated within the canyon. A skimming flow occurs as the H/W increases above 0.7, where the canyon is characterised by circulatory vortices (Oke, 1988). The speed of a single vortex in a skimming flow regime is a function of air flow above the roof level, thermal stratification inside the canyon, and the advective motions from the buildings' corners (Ali-Toudert, 2005). In case of light winds, thermal variations due to the warming of canyon facets can shift the flow from one regime to another (Sini *et al.*, 1996) and a second contra-rotating vortex may be generated (He *et al.*, 2019). Moreover, canyons with an orientation parallel to the wind direction will experience a "channelling effect", whereas those perpendicular to the wind flow will experience transverse flows at the downwind side of the street. An air flow with an oblique angle will result in corkscrew-like eddies along the length of the canyon (Oke, 1988). At a neighbourhood scale, as cities are densified from scattered to compact areas, wind speed and the ventilation potential decrease (He *et al.*, 2019). The heterogeneity of building heights, however, plays an important role in enhancing the ventilation potential, where higher buildings downwash the ambient flow to the street level (Golany, 1996; He *et al.*, 2019).

1.2 Thermal Comfort

Human thermal comfort is already defined as “the condition of mind which expresses satisfaction with the thermal environment”. It is mainly influenced by such bio-meteorological factors as air temperature, radiant temperature, velocity of air, humidity, clothing and metabolic rate production (ASHRAE). Fanger (1972) derived the first expression to indicate both heat and cold stress, the Predicted Mean Vote (PMV), and its corresponding Predicted Percentage of Dissatisfied (PPD) on account of indoor comfort quantification. However, such indices are not as efficient to model the human interaction with their ever-changing outdoor microclimate as they are for the thermoregulatory equilibrium state within an indoor environment. This has led to the development of indices specifically for outdoor comfort evaluation (Potchter *et al.*, 2018). The preceding half-century has seen the development of diverse comfort models in search of a holistic index, capable not only of gauging thermal sensation within warm and cold climates, but also specifying to what extent people perceive

the thermal stress to which they are exposed. Examples are abundant, albeit the most commonly used indices are the Physiologically Equivalent Temperature (PET) (Höppe, 1999) and the Universal Thermal Climate Index (UTCI) (Bröde *et al.*, 2012). These indices provide the full range of thermal sensation, up to ten categories, in hot and cold conditions and provide the equivalent temperature for sensation (Potchter *et al.*, 2018).

UTCI was developed to indicate the air temperature in a reference environment which elicits a similar physiological response to that of the actual environment. UTCI has been developed based on the multi-node Fiala thermoregulatory model (Fiala *et al.*, 2012) which accounts for the dynamic thermal body responses, as well as the advanced clothing model by (Havenith *et al.*, 2012) to account for the adaptation and distribution of clothing. The accuracy of the model stems from the calculation of body thermal and nervous responses in twelve body segments, while at the same time taking into account the inner and outer body heat transfer (Coccolo *et al.*, 2016). UTCI has been applied across all Köppen Geiger climate regions and has been validated against monitored data and other thermal indices, e.g. PET and PMV. Furthermore, UTCI presents a detailed representation of thermal sensation for the neutral as well as the extreme cold and hot conditions (Figure 1) (Blazejczyk *et al.*, 2012). Unlike PMV which sorts thermal stress into categories, UTCI provides the equivalent temperature for sensation in degrees Celsius, which makes it more perceptible by urban designers and planners.

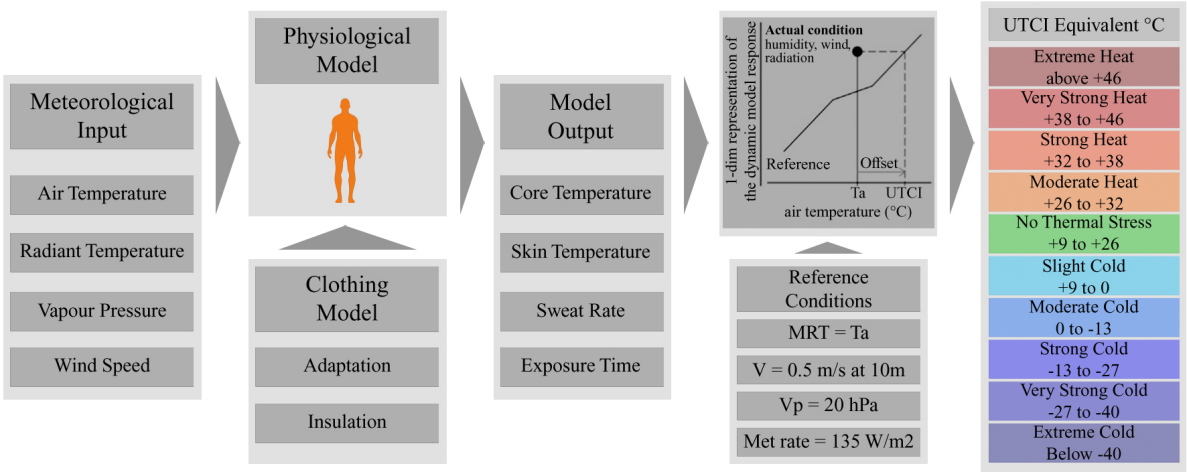

Figure 1: Concept of the UTCI equivalent temperature, adapted from (Bröde *et al.*, 2012)

1.3 Research problem and objectives

Egypt, as a developing country, is striving to contain overpopulation, and provide adequate and affordable housing, whilst also constricting urban sprawl. In 2015, the government set out a long-term action plan for the physical expansion of existing cities, and the planning for new urban communities. However, the endeavours to integrate environmental performance assessment into practice in Egypt are still voluntary. Moreover, the Executive Regulations for the Egyptian Unified Construction Act (Ministry of Housing Utilities & Urban Communities, 2008) specifies merely spatial, rather than climate-responsive urban form design norms and criteria, particularly with respect to the canyon-scale design. This gap between the study of outdoor thermal comfort and the design practice inhibits the improvement of cities' microclimates, thereby deteriorating health and well-being. A number of studies have investigated the impact of canyon geometry design on the microclimate in Egypt. Labib *et al.* (2015) studied the outdoor thermal comfort (represented by PET) of a single urban canyon in Cairo, Egypt, using ENVI-met. The urban canyon however had a fixed street width of 9m, and the simulations ran over only 4 orientations and only 4 height-to-width (H/W) ratios (4 building heights). In their conclusions, the authors pointed out that, timewise, examining a large number of canyon configurations using ENVI-met is cumbersome, and they recommended using a parametric modelling platform that could be efficient to produce a larger number of street configurations. Similarly, Shalaby *et al.* (2018) investigated the microclimate of a simple hypothetical urban layout in Cairo, using ENVI-met. However, the study examined a limited number of canyon configurations, having a street width fixed to 12m and 5 H/W ratios with building heights ranging between 12m and 60m, for different orientations. In their investigation of four urban communities in Cairo, (Galal *et al.*, 2020) claimed that PET at the street level is strongly dependent on the H/W ratio, rather than the mere height or width thereof. However, having a closer look at the H/W ratios examined at this study, only 3 out of 68 streets had a H/W greater than 2. Moreover, none of these studies have considered the performance of asymmetrical urban canyons and if they perform any differently from symmetrical ones.

This paper utilises the parametric design capabilities of modern software packages to be the first to investigate thousands of canyon geometry configurations. The parameters being examined in this study are the street widths, building heights (symmetrical and asymmetrical with respect to the

street axis), H/W ratios and orientation. In this research, our objective is to simulate a wider variety of widths, heights, H/W ratios and orientations to find the optimal urban canyon parameters to improve outdoor thermal comfort and compare these thresholds to those of the Egyptian Construction Act, and then provide recommendations and guidelines that should be adopted in the Executive Regulations. The study is performed in the hot arid climate of Cairo, Egypt, where Cairo accounts for almost 32% of the current new residential projects, and along with Alexandria, around 88% of the residential apartments with air conditioning (CAPMAS, 2019; Mahdy, 2014). In this research, the Ladybug-tools (Roudsari *et al.*, 2020), the plugins for Grasshopper 3D, are used to calculate the UTCI as a metric for outdoor thermal comfort within the street canyon. Also, taking the same approach of the above-mentioned studies, simulations are conducted over a single day that represents severe climatic conditions, which occur during June and July in Egypt.

2 Methodology

The Executive Regulations for the Egyptian Construction Act (Ministry of Housing Utilities & Urban Communities, 2008) specifies some canyon parameter thresholds for urban communities, such as a minimum street width of 10m, maximum building heights of 36m and a maximum H/W ratio of 1.5. Currently, the Egyptian government is considering the applicability of a few amendments to the regulations, with even lower thresholds. Since the aim of this study is to examine a wider variety of H/W's to find the optimum thresholds, the design parameters thresholds were set according to the Executive Regulations (Ministry of Housing Utilities & Urban Communities, 2008), with the exception that street widths were set to a lower bound of 6m (Table 1). A hypothetical urban canyon geometry was created and simulated in three consecutive and correlated phases, with building constructions obtained from Engineering-ToolBox (2001). The first phase includes the simulation of a sole urban canyon, having the building heights on both sides of the canyon (Array A and Array B in Table 1) changing simultaneously to investigate the thermal comfort in symmetric urban canyons, followed by a regression analysis to scrutinise the relationship between the design parameters and the output UTCI. In the first phase, Orientation 180° is anticipated to be identical to orientation 0°. However, it was included to verify the model's performance. The thermal performance (UTCI) of the canyon is assessed

at a single point on the central axis of the canyon at a height of 1.1m to represent pedestrian level thermal comfort, and the outputs of this phase are presented as the average diurnal UTCI recorded from 5 am (sunrise) to 7 pm (sunset). Based on the first phase's results, the thresholds and steps of the parameters are refined in both phases 2 and 3 to those eliciting relatively lower UTCI values (Table 1).

In the second phase, the canyon is simulated within an urban context of an existing newly constructed urban community to provide a more realistic estimation of the urban heat island effect. Heights of the flanking building arrays A & B are varied independently to address the potential of asymmetrical urban canyons for better thermal comfort. The second phase's results are presented as the average value of all points on a 2m grid inside the canyon, rather than a single point. This gives a better overall view of the thermal performance of the canyon and as such avoids any anomalies -if any- of a single point output. The results of this phase are also shown as the average diurnal UTCI recorded from 5 pm to 9 pm (2 hours after sunset) to investigate the impact of solar radiation exposure/blockage on thermal comfort at certain hours. This helps to accentuate the effect of each flank's height on the UTCI and thus supports the design strategies to increase the sky view factor to mitigate the UHI effect; this also helps to interpret the results of the third phase. As per the second phase, in the third phase, building heights are simulated independently, however with fewer steps (Table 1). Results of this phase are averaged across the canyon and presented as the average UTCI registered from 5 am to 7 pm to provide an overall analysis during the daytime. This way, the third phase links the analysis approach of both the first and second phases but with more attention given to each flank's H/W rather than their mere heights. Johansson (2006) investigated the thermal performance of 12 urban canyons in the hot-arid climate of Fez, Morocco, and reported that the relative cooling by day due to shading exceeded the warming by night. For this reason and to better understand the urban geometry response to the solar exposure without being misinterpreted by averaging, nocturnal temperatures were not included in this study.

Table 1: Thresholds and steps of the parameters simulated in all phases.

Phase 1 (a total of 1716 cases)				
	Min	Max	Step	

Building Heights	3m	36m	3m
Street Width	6m	36m	3m
Orientation	0°	180°	15°

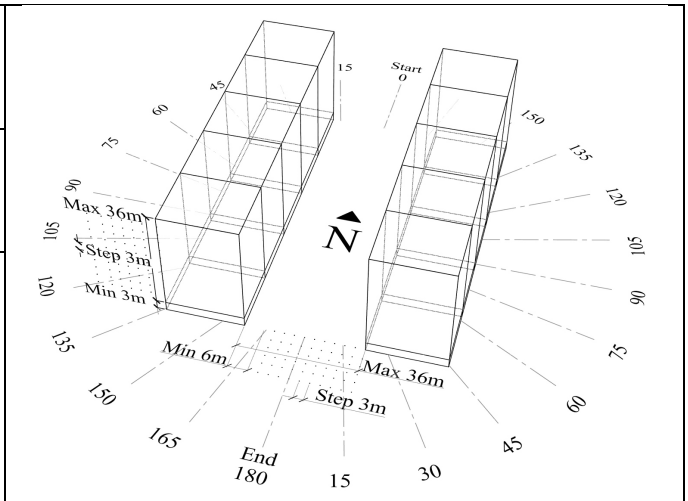

Phase 2 (a total of 3840 cases)

	Min	Max	Step
Building Heights A	8m	36m	4m
Building Heights B	8m	36m	4m
Street Width	6m	18m	3m
Orientation	0°	165°	15°

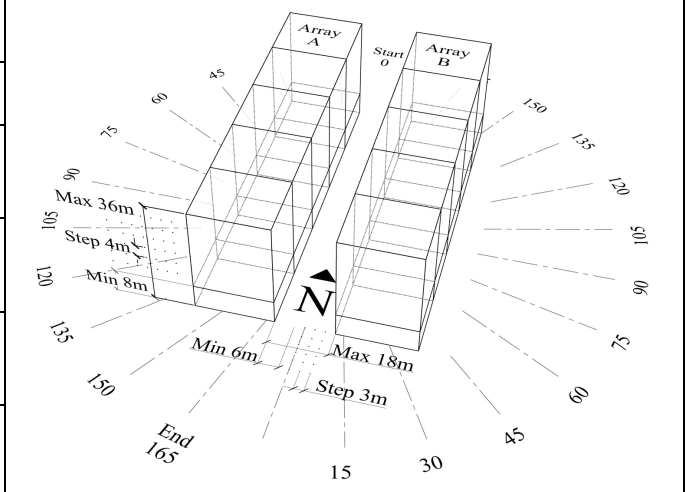

Phase 3 (a total of 2160 cases)

	Min	Max	Step
Building Heights A	6m	36m	6m
Building Heights B	6m	36m	6m
Street Width	6m	18m	3m
Orientation	0°	165°	15°

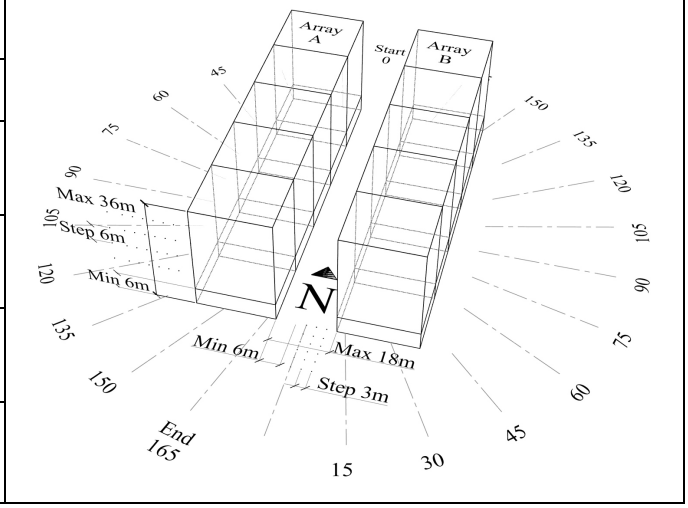

2.1 Simulation workflow

The ladybug-tools model is selected for this study for several reasons; it is considerably less time consuming to perform calculations than ENVI-met, allowing for the simulation of thousands of canyon

configurations, it produces a variety of thermal indices, among them is the UTCI which is the focus of this study, and the ability to parametrically model canyon geometries and to visualise the results within the Grasshopper environment. The ladybug-tools microclimate model is a combination of Grasshopper plugins (Roudsari *et al.*, 2020) used to estimate the outdoor thermal comfort with a graphical representation. The model is based on linking Grasshopper to already validated software engines dedicated to calculating the thermal comfort determinants individually. For instance, Honeybee links Grasshopper to EnergyPlus (Crawley *et al.*, 2001) which calculates the surface temperatures. Dragonfly utilises the Urban Weather Generator (UWG) (Bueno *et al.*, 2013) to calculate the urban air temperature and relative humidity. The algorithm combines a variety of input parameters, such as the average building heights and the surface roughness, to morph the 'rural' weather file into a new 'urban' file containing modified hourly urban air temperatures and relative humidity. Ladybug components are used to visualise the environmental data and the output results. The Butterfly plug-in could potentially integrate OpenFOAM software for CFD air flow analyses, but this would involve prohibitively high computation time. Therefore, wind speeds in this study are retrieved from the weather file, where the weather station 10m-high wind speeds are translated into 2m-high wind speeds and vice versa, where necessary, using a Ladybug component based on the wind profile power law. The mean radiant temperature (MRT) is calculated as the agglomeration of the three components; the long-wave radiation from the surfaces; the amount of the sky long-wave radiation absorbed by the human body; and the additional amount of absorbed solar short-wave radiation. The long-wave radiation from surfaces is estimated by using the following formula:

$$MRT_{Surface} = \left[\frac{\sum_{i=1}^{N} (T_s^4 \cdot F_s + T_e^4 \cdot F_{ns})}{\sum_{i=1}^{N} F_s}\right]^{1/4} \qquad (1)$$

Where T_s is the outside surface temperature calculated by virtue of EnergyPlus. T_e is the ambient temperature of one surface and is assumed to be equal to the ambient air temperature as shaped by the surrounding surfaces. F_s is the view factor between the point of interest and a specific surface and F_{ns} is the non-surface view factor, i.e. view factor to surfaces other than that specific surface. Angle factors are calculated by tracing back the number of spherical vectors impinging one surface and dividing that number by the total number of vectors emanating from each point.

The absorbed sky long-wave radiation is calculated by following the formula specified within the MENEX model (Blazejczyk, 2005) as follows:

$$MRT_{sky}=f_{svv}\cdot\left(\frac{L_a}{\alpha_{lw}\cdot\sigma}\right)^{1/4}-273.15 \qquad (2)$$

Where f_{svv} is the sky view from a certain point unobstructed by opaque surfaces. L_a is the terrestrial sky long-wave radiation, and is obtained from the weather file. α_{lw} is the emissivity of the human body for long-wave radiation (default value of 0.95), and σ is the Stephan Boltzmann constant ($5.667\cdot10^{-8}$ W/m^2K^4). As for the short-wave solar radiation, the model accounts for the absorbed portion by means of the effective radiant field (ERF) specified within the SolarCal model (Arens *et al.*, 2015) and the normative appendix (C) of (ASHRAE) in terms of the three components; the direct; diffused; and reflected solar radiation, where the latter is defined with reference to the global horizontal radiation as follows:

$$ERF_{solar}=\frac{\alpha_{sw}}{\alpha_{lw}}\cdot\left[(0.5\cdot f_{eff}\cdot f_{svv})(I_{Global}\cdot R_{floor}+I_{diff})+(f_p\cdot f_{eff}\cdot I_{Dir})\right] \qquad (3)$$

Where α_{sw} is the absorption coefficient for the short-wave radiation (default value of 0.7), f_{eff} is the fraction of the body exposed to radiation (0.696 and 0.725 for a seated and a standing person respectively). I_{Global}, I_{diff}, I_{Dir} are the global, diffused and direct normal radiation respectively. R_{floor} is the floor/ground reflectivity and f_p is the projected area factor and is derived with reference to the solar altitude and azimuth as in (Fanger, 1972) and (ASHRAE). The amount of additional MRT due to solar radiation is eventually calculated in terms of ERF, f_{eff}, and the radiative heat transfer coefficient (h_r) as follows:

$$MRT_{sol}=ERF_{solar}/f_{eff}\cdot h_r \qquad (4)$$

Figure 2 shows the data streaming between the different plugins, components and simulation engines as used in this study.

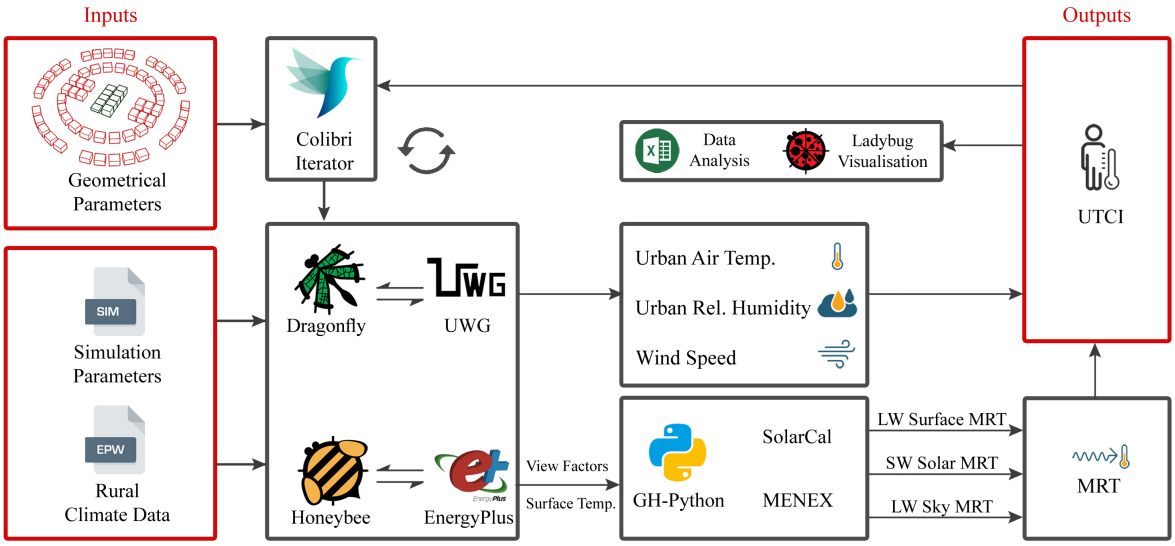

Figure 2: Schematic diagram showing the data streaming between Ladybug-tools plugins and the simulation engines in the workflow used in this study.

2.2 Validation of the workflow

As mentioned in previous sections, the workflow depends on validated software engines to determine the MRT and the thermal comfort components. EnergyPlus was validated with the ASHRAE 1052RP test and verified with a series of building energy simulation programs (BESTEST) as endorsed in ASHRAE Standard 140-2001 as a Standard Method of Test (Witte *et al.*). The UWG was validated with field measurements in different climates (Bueno *et al.*, 2013; Bueno *et al.*, 2014). It is then how the workflow applies the MRT equations and combines the different UTCI components that needs to be validated. A recent study by Evola *et al.* (2020) included the validation of the Ladybug-tools workflow with experimental measurements in a Mediterranean climate context, namely Catania, Italy, in terms of the MRT. Results of that study has shown good agreement with measurements with a coefficient of determination $R^2 = 0.92$. Moreover, in studies by the authors, the workflow has been verified against the CFD modelling package, ENVI-met, in Cairo, Egypt (Ibrahim *et al.*, 2020b), and London, UK (Ibrahim *et al.*, 2020a). Figure 3 shows the results for the average MRT and UTCI of all grid points in

the case of Cairo, having a congruent performance in terms of the MRT and UTCI (R^2 = 0.94 and 0.96 respectively).

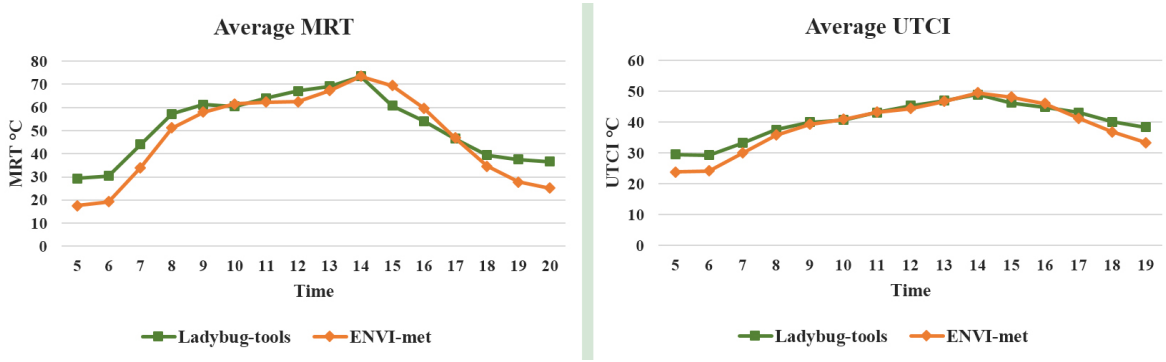

Figure 3: Results for the average of all grid points as simulated by both Ladybug-tools and ENVI-met.

In this study, an urban canyon, located in a university campus in Cairo, was selected to validate the workflow against field measurements (Figure 4-a). The canyon comprises office buildings with a total length of around 50m and asymmetrical H/W of 0.9:1:1.3 and is orientated 42° North-eastwards. The canyon was modelled in Rhino along with the surrounding context of area around 170×110m as shown in Figure 4-b. Construction materials along with their physical and thermal properties were defined in Grasshopper as similar to the real case as possible. A Onset HOBO-U30 (Onset, 2021) weather station and Extech HT30 Heat Stress WBGT Meter (Extech, 2021) were placed at the centre of the street to measure the meteorological parameters needed for validation as shown in Figure 4-c. Table 2 lists the parameters measured in the campaign, the sensors used and their corresponding range and accuracy.

(a) (b) (c)

Figure 4: Site of measurements as shown (a) in Google Earth, (b) in the Rhino scene, and (c) during measurements.

Table 2: The parameters measured by the sensors and their corresponding range and accuracy.

Parameter	Sensor	Range	Accuracy
Air temperature	S-THB-M002	−40 to 75°C	±0.21°C (at 0-50°C)
Relative humidity	S-THB-M002	0 to 100%	±2.5% (at 10-90%)
Wind speed	S-WSB-M003	0 to 76 m/s	±1.1 m/s OR 4% of reading
Black globe temperature	HT30	0 to 80°C	±3°C (Outdoors)

Measurements were recorded on the 6th August, 2018 every hour from 7 am to 7 pm. Measured air temperature (T_a), relative humidity (Rh) and wind speed (v) were compared to their counterparts in an International Weather for Energy Calculation (IWEC) weather file (DoE, 2020), which is used for the simulations in the validation and the rest of this study to check the reliability of the weather file. The mean radiant temperature (MRT) was calculated on site in terms of the black globe temperature (T_g) and the air temperature (T_a) following the formula (British Standards Institution, 2001):

$$MRT = \sqrt[4]{(T_g+273)^4 + \frac{1.1 * 10^8 \times v^{0.6}}{\varepsilon_g \times D^{0.4}} \times (T_g - T_a)} - 273 \qquad (5)$$

Where ($\varepsilon_g = 0.95$) and ($D = 0.04$ m) are the globe emissivity and diameter, respectively. A Honeybee component was used to convert the 10m-high wind speeds from the IWEC file into 2m-high wind speeds and vice versa, required for MRT and UTCI calculations. The latter was calculated by a Ladybug component which takes T_a, Rh, v and MRT and produces the UTCI.

Figure 5 plots the relationship between the measured parameters and their counterparts in the IWEC file. The IWEC parameters appear to be strongly correlated to the measured values with the wind speed having the lowest correlation. This can be explained by the low resolution of the wind speed sensor (0.25 m/s) which resulted in reading (zero m/s) in almost half of the recordings. Even so, the general trends of the three parameters are congruent with the measurements. The relationship between the measured and simulated MRT is shown in the top row of Figure 6, where the simulation workflow appears to be sufficiently reflecting the MRT temporal variations. Based on a sensitivity analysis, the discrepancy in MRT at 10 am can be attributed to the difference between the simulation model and the real site in three main parameters; global horizontal radiation; thermal admittance of the ground surface; and the spatial resolution of the simulation model. Apart from that, the general trend is in agreement with the measurements with maximum difference of 8.01°C. This is in line with previous studies concerning the outdoor thermal comfort and using the same workflow, for instance, 6.1°C in Evola *et al.* (2020) and ~7°C in Naboni *et al.* (2019b).

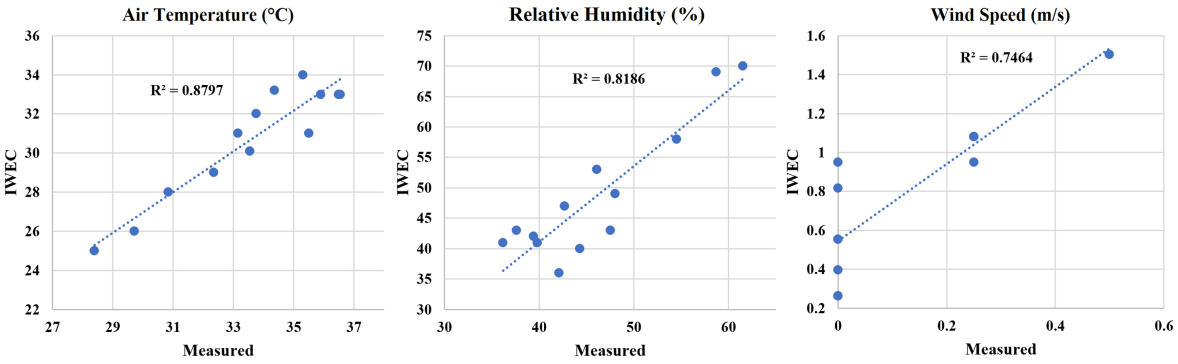

Figure 5: Scattered plots showing the relationship between the measured parameters and the IWEC parameters.

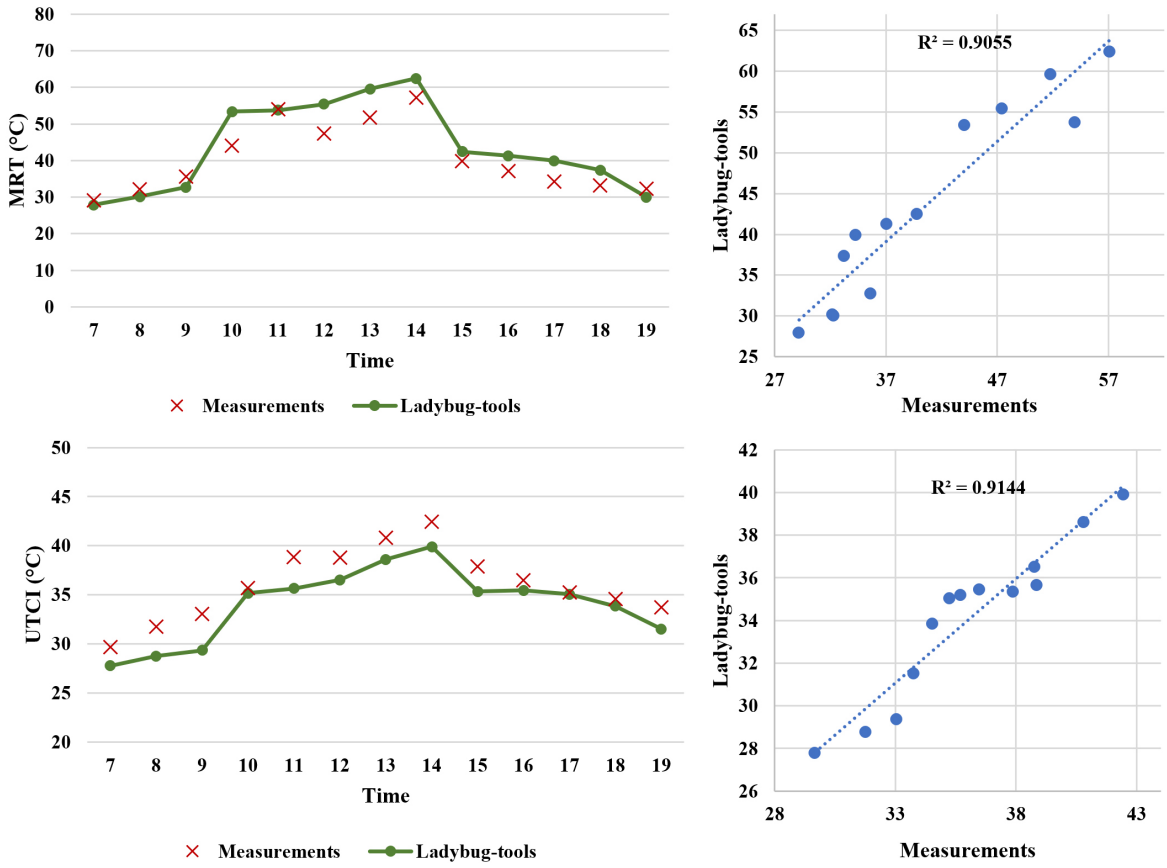

Figure 6: Relationships between measured and simulated MRT (top row) and UTCI (bottom row).

It can clearly be seen that although the parameters, T_a, Rh, and v have some discrepancies with the measured values (Figure 5), the UTCI follows trend of the MRT throughout the day (Figure 6), showing a good agreement with the field measurements UTCI, with a maximum difference of ~3.5°C. The results shown above indicate that the Ladybug-tools workflow can simulate the thermal performance of geometry configurations with a considerable reliability, but also with a comparable accuracy to valid microclimate models such as ENVI-met with dramatically decreased simulation times and hence, it can be used in this study. The results also indicate that the IWEC weather file is adequately appropriate for the simulation of hypothetical case studies. Additionally, the results reported in this validation are not including CFD wind simulation. This was recommended based on a preliminary sensitivity analysis by the authors. Natanian *et al.* (2020) performed a sensitivity analysis on the solar and wind parameters included in the calculation of UTCI using the same workflow in a hot desert climate, similar to our study. Their results showed that MRT had the strongest impact on UTCI, and

that using the wind data from the weather file (rather than a detailed CFD analysis) had a minimal effect on the output UTCI. Also in a hot-arid climate, Krüger *et al.* (2010) concluded that wind exposure is not as significant as mutual shading for improving the heat transfer by convection and reducing cooling loads. Accordingly, based on our preliminary study and the inferences from the literature, and given the exhaustive computation time needed for the CFD analyses, wind speeds in this study are extracted directly from the IWEC file, in favour of performing a total of 7716 permutations.

2.3 Hypothetical study modelling

The hypothetical urban canyon, comprised of two arrays of 5 residential units, 24m × 20m each, was modelled parametrically in Grasshopper (100m total canyon length). The ground in the ladybug-tools model was defined as a thermal zone in EnergyPlus in order to account for ground temperature changes. The ground zone was further divided into 5 zones during the first phase and 20 zones during the second and third phases, to capture the dynamic variation of the shading without increasing the computation time. Building materials typical of the residential sector in Egypt were defined as the construction materials for the model, with all material roughness set to "rough". Table 3 lists the thermal and physical properties used in this study. Upon the second and third phases, an existing newly constructed urban area in Cairo is modelled with average building heights of 18m are assumed. Note that the UWG module within the Dragonfly plugin uses the average building heights, building footprints, density and material thermal properties to calculate the UHI effect. Since the context neighbourhood is not orientated with the urban canyon, the morphology and the spacing between neighbouring buildings will not affect the results of the UWG. Figure 7-a depicts the canyon as modelled in phase 1, while Figure 7-b and Figure 7-c show the canyon as modelled within the context neighbourhood and used in both phases 2 and 3.

Table 3: Physical and thermal properties of construction materials (Engineering-ToolBox, 2001).

Material / Properties	Roofs	Walls	Ground
	Roofing tiles	**Wall bricks**	**Asphalt**
Solar Absorption (-)	0.50	0.60	0.88
Solar Reflection / albedo (-)	0.50	0.40	0.10
Thermal Absorptance (-)	0.90	0.90	0.93
Density (Kg/m^3)	1900	1500	2100
Specific Heat Capacity (J/Kg·K)	800	650	920
Thermal Conductivity (W/m·K)	0.84	0.44	1.40

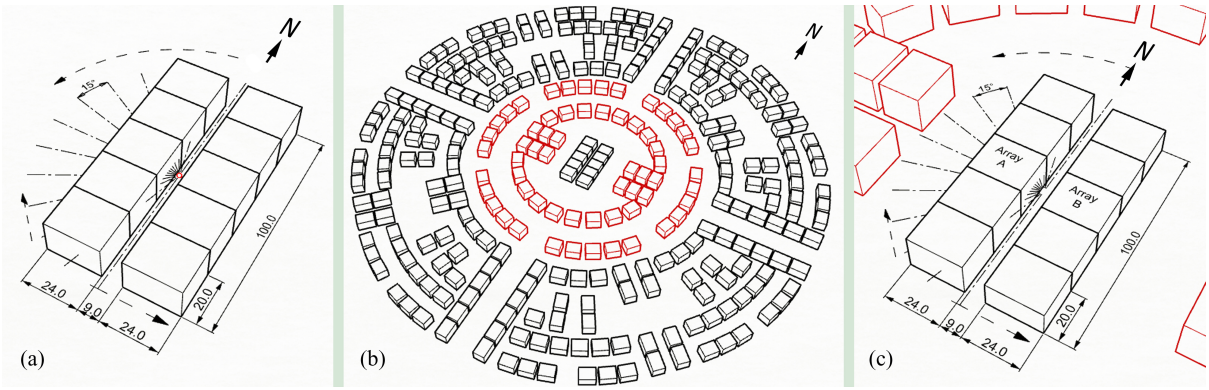

Figure 7: 3D view of the urban canyon simulated in (a) phase 1, and (b) and (c) in both phases 2 and 3. Neighbouring buildings in red colour are included in the view factor calculations.

2.4 Simulation setup

For the Dragonfly Urban Weather Generator inputs, a building programme was set to "mid-rise apartments". For the parameterisation of EnergyPlus simulation via Honeybee, each building was divided into a number of thermal zones equal to the building's floors, i.e. one thermal zone per floor, to capture the variations in surface temperatures relative to the dynamic shading pattern. Building zones were set to "not conditioned", with equipment and lighting loads set to zero. In the same context, the timestep was set to 10 mins with reporting every hour, and using the solar distribution module "Full exterior with reflections". The points of measurements were distributed along the canyon on a 2m grid, e.g. a 100m long street of width 6m entails a total of 50×3=150 points. Results were recorded at a height of 1.1m to represent the centre of gravity of a human body, thus taking a thermal sensation point of view. For phase 2 and 3, the nearest neighbouring buildings (shown in red colour in Figure 7-b) are included for view factor calculations, yet not for shadowing. The TT-Toolbox (Tomasetti, 2020) Colibri component was used to iterate a total of 1716, 3840 and 2160 cases respectively for the first, second and third phases.

2.5 Climate context

Egypt encompasses a range of diverse climatic conditions; however, it is generally categorised as a hot-desert climate according to the Köppen Geiger classification. The climate is characterised by a

hot-arid summer and a temperate winter with low precipitation levels. The highest mean temperatures are typically in July while the coldest temperatures are in January. An International Weather for Energy Calculation (IWEC) file for Cairo was obtained from the U.S. DoE (2020) and used in this study. Simulations, however, were conducted on June 7th as the hottest day to represent the worst-case scenario. Figure 8 shows the meteorological data of June 7th that were input into the simulation. It's clear that the radiation values are not typically symmetrical around noon. Consequently, the performance of canyons providing similar shading patterns across the day will slightly vary based on the radiation values that they receive and/or block, as discussed below.

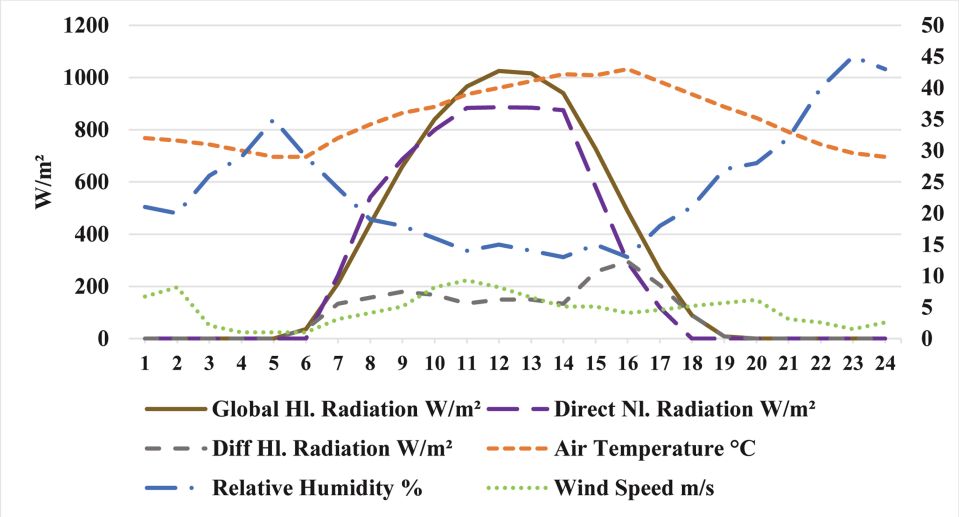

Figure 8: Meteorological data in Cairo, on June 7th, as retrieved from the IWEC file and input to the model.

3 Results and discussion

For symmetrical canyons in phase 1, besides showing the optimum H/W ratios within each orientation, a focus is given to allocating specific heights and widths that produce these optimum ratios, where different height and widths may produce the same H/W. In phase 2, asymmetrical canyons are analysed with more emphasis on the heights of each array of buildings (flank). In phase 3, the heights of each flank within different widths are analysed with more attention to each flank's H/W. This set of analyses gives a comprehensive interpretation of the relationship between design parameters and the output thermal comfort.

3.1 Phase 1

Results of the first phase were interpolated using 2D Non-Uniform Rational Based Spline (NURBS) surfaces, and then transformed into coloured meshes, with each face delineating a resultant UTCI value of using a certain street width and building height as shown in Figure 9. Results of orientation 180° were excluded since they showed identical performance to those of orientation zero, as expected. In general, it can be noted that higher H/W ratios within all orientations lead to the lowest UTCI. However, N-S, NW-SE (15-45°) and NE-SW (135-165°) orientations tend to produce a wider variety of lower UTCI H/W ratios than those orientations close to E-W (60-120°). Given that the solar altitude reaches ~82° at noon, E-W canyons remain exposed almost the entire day and thus maintain the highest UTCI values.

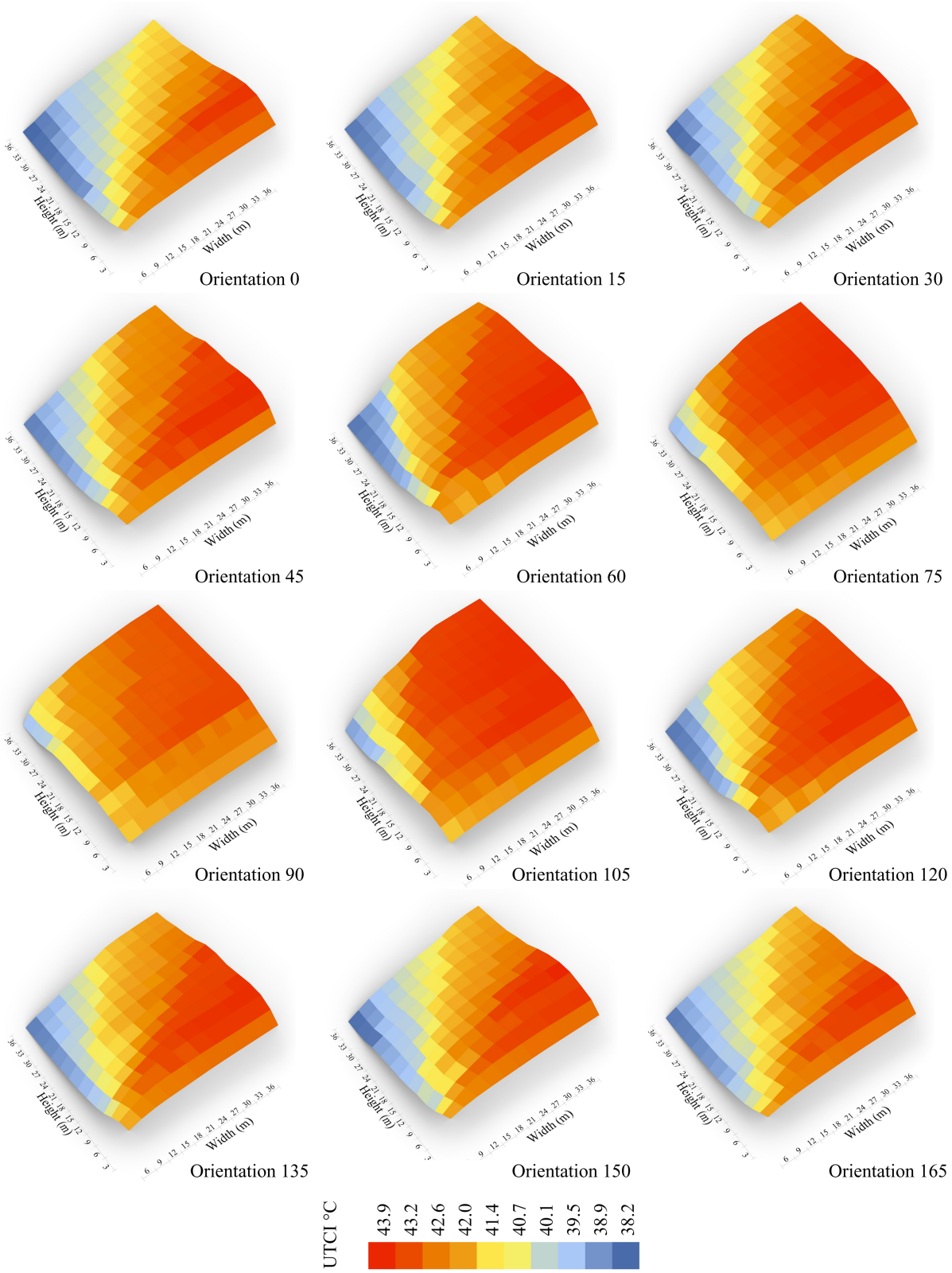

Figure 9: Coloured meshes showing the height-to-width based UTCI for different orientations in degrees relative to North, recorded in the middle of the canyon on June 7th, from 5 am to 7 pm.

The more E-W orientated the canyons are, the less impact the street widths have on the UTCI. This is attributed to the longer exposure time not only for the canyon ground but also for the building surfaces, hence, the taller the buildings within these canyons, the more long-wave radiation a receptor point receives. Also, NE-SW canyons (120, 135 and 150°) having H/W ratios between 1 and 1.5 (Figure 9) tend to be a preferred orientation relative to their NW-SE counterparts (60, 45 and 30°). Despite both NE-SW and NW-SE spending almost the same time sun-exposed or shaded, NE-SW canyons provide shading during the morning hours, obstructing radiation values relatively higher than those in the late afternoon. As canyon ground starts to heat up around 9 am, NW-SE canyons, on the other hand, provide shading during the late afternoon hours where surfaces are already heated, and the shading effect is lessened. Also, canyons within orientation 90° showed slightly better performance than those within orientation 75 and 105° with streets wider than 12m, as the former casts more shading during the noon hours (12-1 pm) characterised by the highest solar radiation intensities. Results of this phase are in agreement with previous studies in hot arid climates (Ali-Toudert *et al.*, 2005; Ali-Toudert *et al.*, 2006; Bourbia *et al.*, 2010; Galal *et al.*, 2020; Johansson, 2006; Shalaby *et al.*, 2018) which advocated the use of NS-oriented deeper canyons for better thermal conditions.

Heights	6	9	12	15	18	21	24	27	30	33	36
36	6.00	4.00	3.00	2.40	2.00	1.71	1.50	1.33	1.20	1.09	1.00
33	5.50	3.67	2.75	2.20	1.83	1.57	1.38	1.22	1.10	1.00	0.92
30	5.00	3.33	2.50	2.00	1.67	1.43	1.25	1.11	1.00	0.91	0.83
27	4.50	3.00	2.25	1.80	1.50	1.29	1.13	1.00	0.90	0.82	0.75
24	4.00	2.67	2.00	1.60	1.33	1.14	1.00	0.89	0.80	0.73	0.67
21	3.50	2.33	1.75	1.40	1.17	1.00	0.88	0.78	0.70	0.64	0.58
18	3.00	2.00	1.50	1.20	1.00	0.86	0.75	0.67	0.60	0.55	0.50
15	2.50	1.67	1.25	1.00	0.83	0.71	0.63	0.56	0.50	0.45	0.42
12	2.00	1.33	1.00	0.80	0.67	0.57	0.50	0.44	0.40	0.36	0.33
9	1.50	1.00	0.75	0.60	0.50	0.43	0.38	0.33	0.30	0.27	0.25
6	1.00	0.67	0.50	0.40	0.33	0.29	0.25	0.22	0.20	0.18	0.17
3	0.50	0.33	0.25	0.20	0.17	0.14	0.13	0.11	0.10	0.09	0.08
	6	**9**	**12**	**15**	**18**	**21**	**24**	**27**	**30**	**33**	**36**

Widths

Figure 10: H/W matrix as a product of all building heights and street widths in phase 1.

The lowest UTCI values of less than 39°C were recorded for canyon heights of ≥18m within 6m streets and heights of ≥27m within 9m streets (H/W ranging between 3 and 6) within all orientations other than E-W canyons (75, 90 and 105°). The latter registered lower UTCI, of less than 40°C, with

building heights of 27m or more on a 6m street with H/W between 4.5 and 6. Canyons close to N-S orientation (0, 15 and 165°) start to register their highest UTCI values, ≥43°C, as building heights decrease to ≤15m within 18m and wider streets so long as they have H/W ratios between 0.16 and 0.45, respective to their parameters. Whereas NW-SE (30 and 45°) and NE-SW (135 and 150°) canyons register their highest UTCI, ≥43°C, as building heights decrease to ≤21m, street widths increase to ≥15m, so long as they have H/W ratios between 0.16 and 0.66, respective to their parameters (Figure 10). Within orientations (60° and 120°), the ratios move to ≤30m height and ≥12m width with H/W between 1.6 and 0.9, respective to their parameters. On the other hand, E-W canyons register UTCI higher than 43°C as building heights increase above 6m (except for 9m in 90°) within 12m streets and wider so long as they have H/W ratios between 0.16 and 1.67, respective to their parameters (Figure 10). Table 4 lists the lower and higher bounds for the geometry parameters, within which minimum and maximum UTCI values were registered.

Table 4: Upper and lower bounds for geometry parameters to produce minima and maxima UTCI.

	Minima UTCI (<39°C) *						Maxima UTCI (>43°C)					
Parameter	Heights (m)		Widths (m)		H/W		Heights (m)		Widths (m)		H/W	
Bounds	Min	Max	Min	Max	Min	Max	Min	Max	Min	Max	Min	Max
0, 15, 165°	18	36	6	9	3	6	6	15	18	36	0.16	0.45
30, 45, 135, 150°	27	36	6	9	3.6	6	6	21	15	36	0.16	0.66
60, 120°	24	36	6	9	4	6	6	30	12	36	0.16	0.9
75, 90, 105°	27	36	6	6	4.5	6	6	36	12	36	0.16	1.67
* <40°C in case of 75, 90 and 105°												

Having a closer look at Figure 9 and Figure 10, it should be noted that canyons with different heights (H) and widths (W) albeit with the same H/W may produce different UTCI values, in contrast to the findings previously reported by (Galal *et al.*, 2020). For instance, an urban canyon with H6 and W12 (H/W = 0.5) produces lower UTCI than a canyon with H9 and W18 by 0.8°C and 1.2°C in orientations 0 and 60°, respectively, and lower than a canyon with H12 and W24 by 1.1°C in orientation 90°. A regression analysis for a sample size of 1716 cases was conducted to distinguish the effect of urban form variables in symmetric urban canyons as in this phase. A 2nd order polynomial trendline was used as it has shown the best fit with the sample data. Of the different variables investigated, H/W and sky view factor had the most significant correlations with UTCI with R^2 = 0.71 and 0.73, respectively

(Figure 11), compared to 0.48 and 0.44, reported by (Galal *et al.*, 2020). When orientations 60 to 120° were excluded from the authors' analysis, a stronger correlation was found for the H/W with $R^2 = 0.91$, compared to 0.56, also reported by (Galal *et al.*, 2020). Furthermore, the authors also found a moderate correlation between UTCI and street widths with $R^2 = 0.49$. This indicates that having a wider variety of canyon parameters in our study allows a more precise estimation of the relationship between urban form and thermal comfort, and identifies new relationships not previously reported, highlighting the significance of this study.

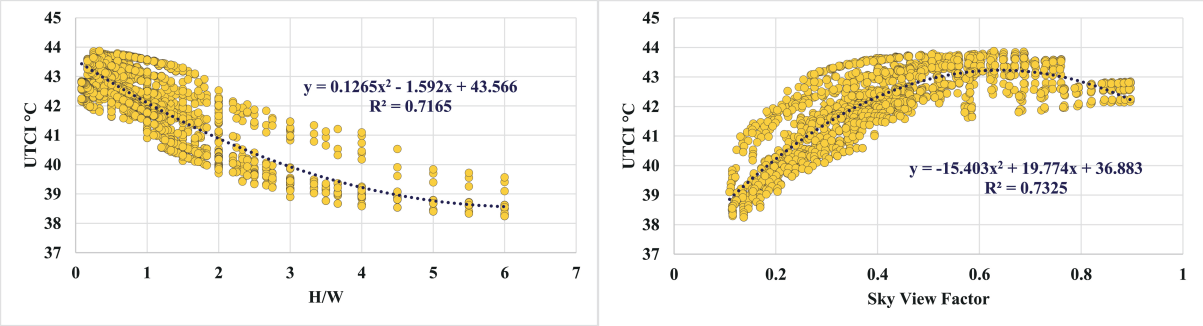

Figure 11: scattered plots for the correlation between UTCI and H/W (left) and sky view factor (right).

3.2 Phase 2

Results of phase 2 show that the lowest UTCI values are a product of the narrowest streets and the highest buildings and vice versa. Consequently, results are shown in Figure 12 as clustered columns, each of which presents the variation of heights of array B with respect to each height of array A within a street width of 6m. Error bars represent the worst cases, within a street width of 18m, which generally produces the highest UTCI values, except for orientations 75, 90 and 105° within 8m-high array A. It is worth noting that although the results of this phase are only presented for 5 pm to 9 pm, EnergyPlus calculation of surface temperatures ran over the whole day. Consequently, surface temperature deviations during the morning and early afternoon hours should be taken into consideration. On a 6m wide street, a general trend can be seen within all orientations; UTCI values decrease with increasing the heights of array A. The effect is clearly seen within orientations where array A faces the southwest direction (45, 60 and 75°). In a similar vein, the effect of increasing the heights of array B is more prominent beyond orientation 90°. It is worth mentioning that although the turbulent heat fluxes are not

considered in the model, the natural convective heat transfer coefficient in EnergyPlus is based on the surface temperature variance with the air temperature, in addition to the wind speed, which is consistent over the whole layout. Given the disparate surface temperatures from one building height to another, heat transfer by convection becomes proportional to the mean difference between the surface and air temperature. In other words, the higher the surface temperature, the higher the natural convective heat transfer coefficient. Consequently, as buildings move from lower heights (exposed with high surface temperature) towards higher building heights (shaded with lower surface temperature), the natural convective heat transfer coefficient diminishes, and so does the heat transfer by convection. Thus, differences between higher buildings (28-36m) tend to be minimal as opposed to those between lower buildings (8-24m). In the next four sections, building heights are referred to by joining the array character “A or B” with its corresponding height in meters. For instance, “A-16 and B-32” indicate 16m-high array A and 32m-high array B.

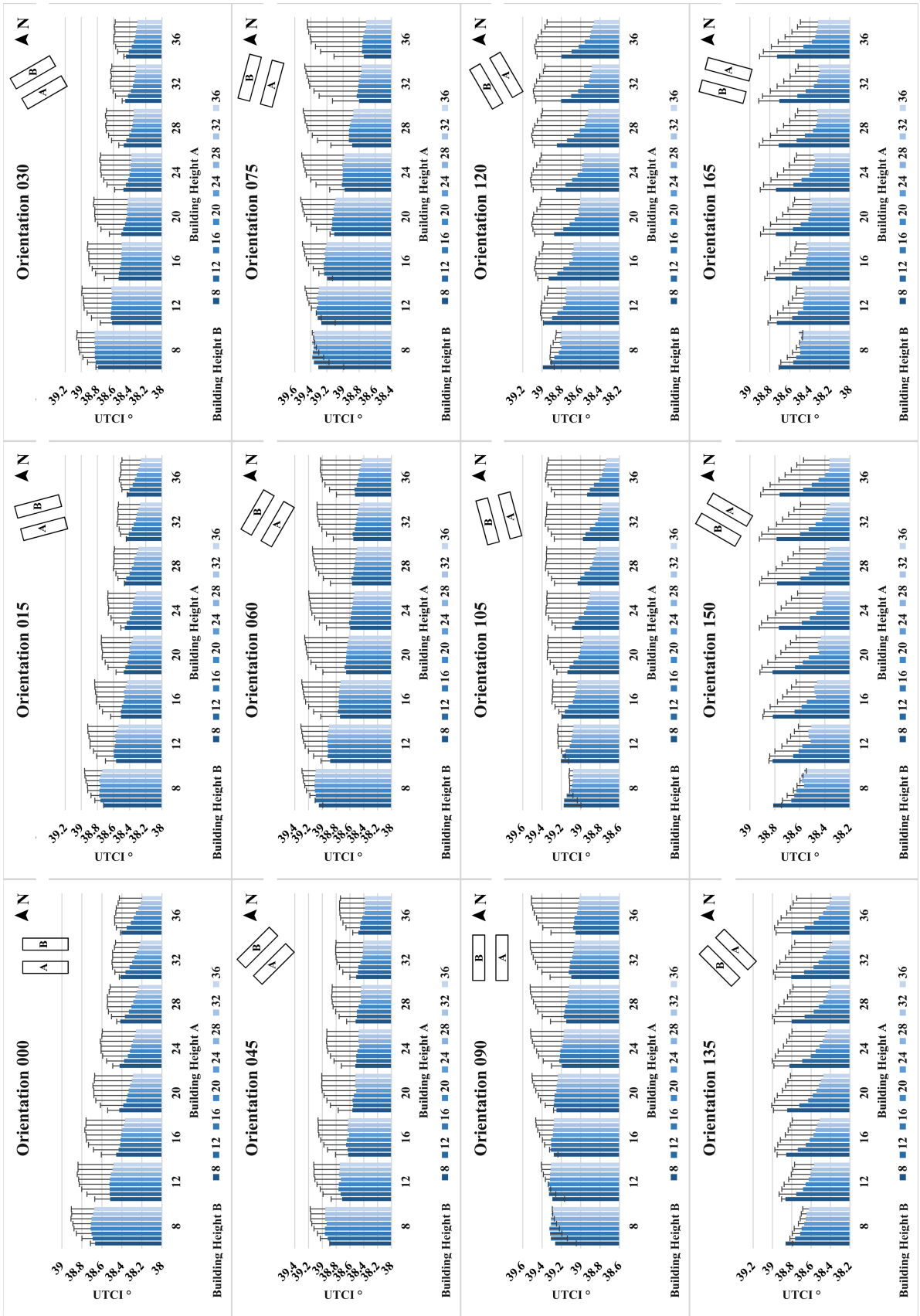

Figure 12: Clustered columns showing the relationship between building heights of array A and array B. The (thick) blue columns represent a 6m wide street, while the (ticked) error bars represent an 18m wide street.

3.2.1 Orientations 0-30°

Within these orientations, the effect of array B on reducing UTCI starts to be clear with increasing array A (20m onwards) for narrow streets. Increasing array B (except for heights B-32 and B-36) in tandem with array A-8 and A-12 increased the UTCI through increased long-wave radiation more than they decrease it by shading. For the same reason, increasing array B on wide streets (18m) resulted in increasing UTCI within arrays A-8 up to A-20, while the effect is attenuated within arrays A-24 up to A-36 due to the combined shading of arrays A and B. Table 5 shows the minimum and maximum UTCI values relative to their canyons on 6m and 18m streets for the three orientations.

Table 5: Minimum and maximum UTCI for orientations 0-30°.

	Max UTCI °C		Max Canyon		Min UTCI °C		Min Canyon		Attenuation °C (Max-Min)	
	6m	18m	6m	18m	6m	18m	6m	18m	6m	18m
0°	38.71	38.89	A8/B20	A8/B24	38.19	38.41	A36/B36	A36/B8	0.52	0.50
15°	38.78	38.96	A8/B16	A8/B36	38.26	38.43	A36/B36	A36/B8	0.52	0.53
30°	38.84	39.06	A8/B28	A8/B32	38.30	38.47	A36/B36	A36/B8	0.53	0.58

3.2.2 Orientations 45-75°

The behaviour of these orientations is dominated by array A blocking solar radiation in the late afternoon and evening. This can be seen through the reductions in UTCI being registered with increasing heights of array A within narrow streets. Increasing the heights of array B appears to increase the UTCI within arrays A-8 to A-16, have a minimal effect within arrays A-20 and A-24, and then decrease the UTCI within arrays A-28 to A-36, especially B-24 and higher. Conversely, on wider streets (18m), lower heights of array B led to a reduction of the UTCI within all heights of array A. Similar to orientations 0-30°, this is attributed to the long-wave radiation received from array B and the lack of shading from array A. However, angle factors between the points of measurements and the surfaces play an important role in shaping the UTCI, particularly in orientation 75°. This is clear in canyon A-8/B-8 where the points have a lower view factor to the surfaces, regardless their temperatures, and hence register a lower UTCI than those of A-36, provided that array B has a minimal shading effect over the

whole day. Table 6 shows the minimum and maximum UTCI values relative to their canyons on 6m and 18m streets for the three orientations.

Table 6: Minimum and maximum UTCI for orientations 45-75°.

	Max UTCI °C		Max Canyon		Min UTCI °C		Min Canyon		Attenuation °C (Max-Min)	
	6m	18m	6m	18m	6m	18m	6m	18m	6m	18m
45°	38.96	39.18	A8/B16	A8/B36	38.38	38.56	A36/B32	A36/B8	0.58	0.61
60°	39.11	39.31	A8/B24	A12/B36	38.43	38.80	A36/B36	A36/B36	0.69	0.51
75°	39.38	39.52	A8/B28	A20/B36	38.71	38.99	A36/B36	A8/B8	0.67	0.53

3.2.3 Orientations 90-120°

For orientation 90°, the UTCI is driven by mutual shading between array A and B. Within narrow streets, increasing heights of array A starts to have an impact on the UTCI at A-24 onwards. This is also the case for array B. This is due to the shading cast by array A during the early afternoon hours (12 pm – 3 pm) and that casted by array B during the late afternoon (4 pm – 7 pm). As streets get wider, the points of measurement receive a negligible amount of shading compared to the long-wave radiation they receive from the building surfaces, thereby increasing the UTCI. As canyons move north-eastward (Orientations 105-120°), array B starts to cast shadow during the late afternoon and alleviates the UTCI regardless the height of array A. Even within wider streets (18m), where increasing heights of array A increase the UTCI, array B alleviates the UTCI as it increases beyond 24m. Table 7 shows the minimum and maximum UTCI values respective to their canyons on 6m and 18m streets for the three orientations.

Table 7: Minimum and maximum UTCI for orientations 90-120°.

	Max UTCI °C		Max Canyon		Min UTCI °C		Min Canyon		Attenuation °C (Max-Min)	
	6m	18m	6m	18m	6m	18m	6m	18m	6m	18m
90°	39.34	39.52	A12/B20	A32/B36	39.02	39.05	A36/B36	A8/B8	0.32	0.48
105°	39.20	39.37	A12/B8	A32/B20	38.74	39.00	A36/B36	A8/B8	0.47	0.37
120°	38.99	39.12	A8/B28	A24/B16	38.46	38.85	A36/B36	A8/B36	0.53	0.27

3.2.4 Orientations 135-165°

It is clear that the effect of increasing heights of array B is predominant due to keeping canyons of all widths shaded. Given the lower solar altitude from 5 pm to 7 pm (~22°), the shading effect extends to wider streets. Array A appears to have a minimum effect on the UTCI due to the shading it provides during the early and noon hours. However, the wider the street, the larger the difference between the long-wave radiation it delivers, and the shading benefits it provides. This is similar to the effect of array B within orientations 45-90°. The impact of array B is more pronounced when it is shaded by array A before 3 pm, especially within orientations 150 and 165° in 6m streets. Table 8 shows the minimum and maximum UTCI values relative to their canyons on 6m and 18m streets for the three orientations.

Table 8: Minimum and maximum UTCI for orientations 135-165°.

	Max UTCI °C		Max Canyon		Min UTCI °C		Min Canyon		Attenuation °C (Max-Min)	
	6m	18m	6m	18m	6m	18m	6m	18m	6m	18m
135°	38.87	39.01	A12/B8	A20/B12	38.38	38.69	A36/B36	A8/B36	0.48	0.32
150°	38.82	38.92	A16/B8	A24/B8	38.35	38.55	A32/B36	A8/B36	0.46	0.38
165°	38.74	38.91	A16/B8	A32/B8	38.30	38.47	A32/B32	A8/B36	0.44	0.44

3.3 Phase 3

Results of this phase are presented as the average UTCI for each 6 heights of one flank against a single height of the other flank, e.g. the average of 6 UTCI values as a product of 6 heights of A (A-6 up to A-36) against B-12. This demonstrates the effect of a single height of one flank regardless the other heights of the other flank. The averages of flank A (single B) are shown in green columns in Figure 13 for 5 street widths, while the averages of flank B (single A) are shown as dash-lined columns. In N-S canyons (0, 15, 165, 30 and 150°), the effect of increasing the height of one flank within an orientation (15° for instance) is contrary to the effect of increasing the same flank within its supplementary orientation (165°). In NW-SE (45, 60 and 75°) and NE-SW (135, 120 and 105°) canyons, the effect is almost similar, though the magnitude slightly differs depending on the hours of the day being exposed/blocked as discussed in phase 2. As streets get wider, UTCI increases for all heights of flank B. On the other hand, for A-6, a street width of 15m (W15) entails lower UTCI than W12 in orientations 30, 45, 135, 150 and 90° and so does W9 than W6 in orientations 60, 75, 105 and 120°. This is due to

the reduced amount of longwave radiation received as streets get wider and the surface view factors decrease accordingly.

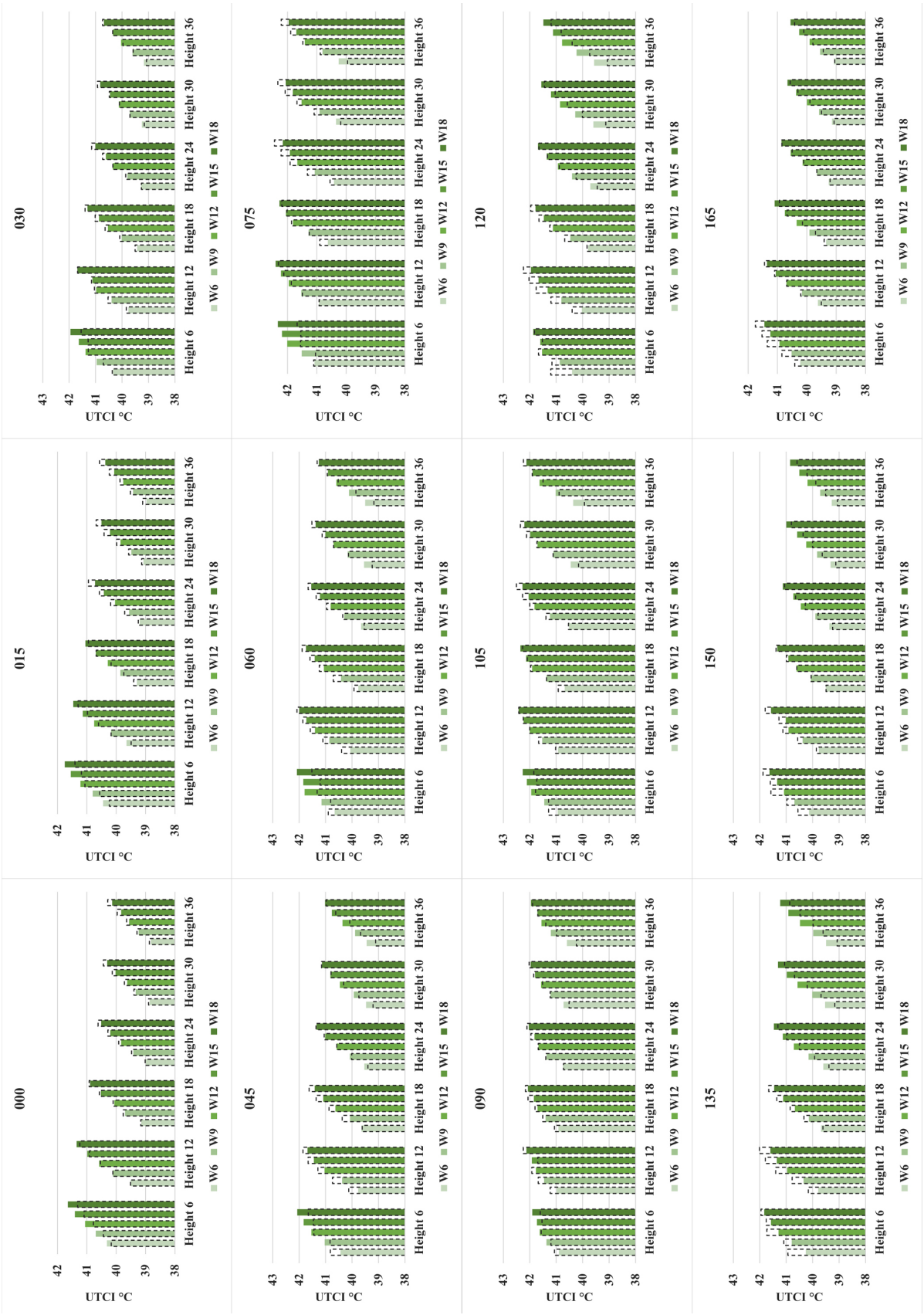

Figure 13: Clustered columns showing the average UTCI for 6 heights of flank A against one height of flank B in (green) and the average for 6 heights of B against a single height of A in (dash lines), within 5 street widths.

Moreover, results of this phase demonstrate how the magnitude of UTCI is dependent on the heights of flanks A and B and the different widths in N-S, NE-SW and NW-SE canyons more than it is in E-W canyons. As such, within E-W canyons, the effect of heights is negligible compared to that of changing the width. Apart from orientations 0, 15 and 75°, heights A-30 and A-36 lead to the minimal UTCI in street widths W6 and W9. This was clear when we investigated the correlation of Heights-A/W and Heights-B/W independently across the different orientations (Figure 14-a and Figure 14-b), and then within each orientation (Figure 14-d). It was found that Height-A/W has a relatively higher correlation with UTCI than Height-B/W (R^2 = 0.44 compared to 0.38). Figure 14-d demonstrates that within orientations 120 to 165°, heights of A had a strong correlation with UTCI compared to a moderate correlation of heights B. Also, in orientations 75 and 90°, flank A had relatively higher correlation than flank B. This is due to being flank A responsible for blocking the solar radiation during most of the sunlit hours. Hence, improved thermal comfort can be achieved by increasing the heights of the southern flank (A in this case) and maintaining lower heights of the northern one (B). This is different from what has been reported in the study of (Shalaby *et al.*, 2018), which recommended using H/W = 1 in E-W canyons, the difference being that they did not include asymmetrical urban canyons in their study. Furthermore, Figure 14-c and Figure 14-d manifest the importance of using each flank's H/W rather than using an average H/W in asymmetrical urban canyon studies, even if the latter maintains a good correlation with the output thermal comfort. Note that the asymmetrical nature of the other meteorological variables around midday may have overestimated or underestimated the output UTCI. However, urban shading remains the most dominating factor in determining the relationship between each flank and the output thermal comfort (also see Emmanuel *et al.*, 2007). Again, having both canyon flanks modelled independently has allowed the examination of the nuances of their relationship with the outdoor thermal comfort, highlighting another contribution of this study.

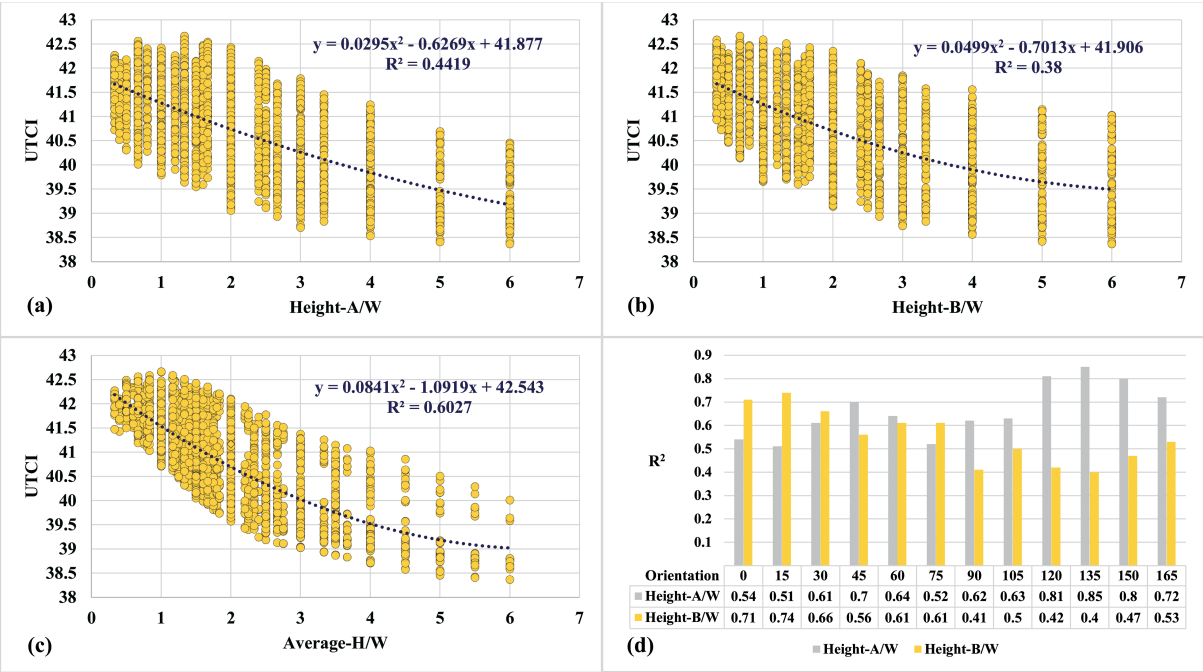

Figure 14: Scattered plots showing the correlation between UTCI and (a) height-A/W, (b) height-B/W, (c) average-H/W. (d) coefficient of determination for height-A/W and height-B/W in different orientations

4 Implications for urban design

As mentioned earlier, the Egyptian Construction Act (Ministry of Housing Utilities & Urban Communities, 2008) specifies urban form thresholds for urban communities; a minimum street width of 10m, maximum building heights of 36m, a maximum H/W of 1.5 and even lower thresholds for new conurbations. Since the results of this study fall within the same UTCI category, we set the benchmark for UTCI reduction as the difference between the highest UTCI recorded and the lowest UTCI resulting from using a H/W of 1.5. Consequently, a reduction in UTCI of 3.7 °C and 2.6 °C were set as the benchmarks for phase 1 and 3, respectively. Table 9 lists the minimum H/W thresholds to meet these reduction benchmarks in both symmetrical and asymmetrical configurations. Note that since the study was conducted on the hottest day, the thresholds are still appropriate for less severe conditions. Based on these findings, higher H/W's and narrower streets should be allowed within the regulations. Street widths 6 to 9m should be orientated E-W wherever possible to serve as local and sub-local roads, or pedestrian alleys. Wider streets should be orientated N-S wherever possible to serve as collectors, whereas intermediate orientations could serve as both. It can be deduced that higher and medium H/W

ratios lead to relatively low and moderate heat stresses in NS, NE-SW and NW-SE canyons. Within these canyons, wider streets with varying building heights can still yield lower heat stresses relative to the other orientations. This is useful for leveraging the solar radiation in winter and allowing air movement for better convective cooling in summer (Qaid *et al.*, 2015).

Table 9: Minimum H/W thresholds for achieving the UTCI reduction benchmarks.

	Orientation											
	0	15	30	45	60	75	90	105	120	135	150	165
Symmetrical H/W	1.67	2	2	2.25	2.5	4.5	5	4.5	2.5	2	1.5	2
Asymmetrical H-A/W	0.67	1	2	2	2.67	5	6	5	2.67	2	2	1.3
Asymmetrical H-B/W	1	1.3	1	1	1	3	5	3	1	1	1	1

Based on the results of the first and third phases, a "UTCI rose" is presented to help draw implications for urban designers, planners and decision-makers as a guideline for a lower heat stress urban environment during the early design stages. Figure 15 depicts the results of both phases, summarised in three bars within each orientation. The left-hand bars represent the resultant UTCI due to increasing or decreasing both canyon flanks' H/W ratios. The middle and the right-hand stacked bars represent the resultant UTCI from increasing or decreasing the canyon flanks A and B respectively, within different street widths. In these stacked bars, the UTCI results are averaged for each 6 heights of one flank with respect to every single height of the other flank. The effect of increasing either building arrays in NS canyons is almost equivalent. In NE-SW canyons, the resultant UTCI is more dependent on the southern array (B in the rose) than it is on the northern array (A). Increasing the heights of the southern array (B) decreases the UTCI relatively more than array A does, although the lower heights of array B lead to higher UTCI than their counterparts in array A. The difference is attenuated as canyons are directed NS, however with slightly higher UTCI values in the lower heights of array B, owing to the higher solar radiation values in the morning and noon compared to the afternoon and evening. The opposite conditions are evident in NW-SE canyons. Canyons close to E-W, on the other hand, maintain relatively higher heat stresses across the majority of their H/W ratios, apart from the highest ones (narrowest streets). Within these canyons, increasing the heights of the northern array is only beneficial as long as they are shaded by the southern array. This is clear in wider streets (15 and 18m), where

building heights 12 to 18m of the southern array lead to higher UTCI than that of height 8m. In the latter case, canyon shading can be achieved by artificial shading devices, galleries (Ali-Toudert *et al.*, 2007) or tree lines (Fahmy *et al.*, 2018). As the southern array increases above 18m, the UTCI starts to decrease again, and it further decreases as streets get narrower. It also can be suggested that, of the heights being tested in phase 3, an 18 to 24m-height of the southern array in E-W canyons works as a trade-off between solar penetration in winter and thermal loads induced within different street widths.

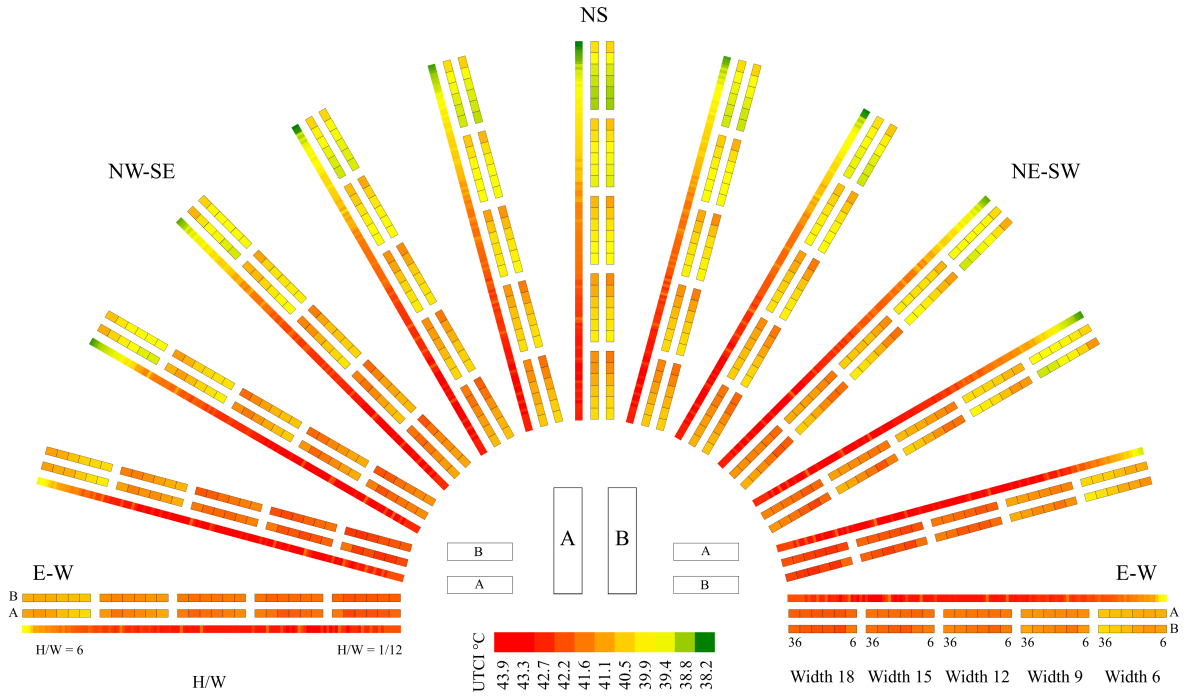

Figure 15: UTCI rose. For each orientation, left-hand bars represent 132 H/W ratios and their resultant UTCI. Within the 5 street widths, middle stacked bars represent 6 heights of flank A along with their resultant UTCI as averaged over each respective 6 heights of flank B. Right-hand bars represent 6 heights of flank B along with their resultant UTCI as averaged over each respective 6 heights of flank A.

The methodology presented in this paper can be replicated and used to test other performance criteria, e.g. energy loads, by means of its core simulation engine, EnergyPlus (Ibrahim *et al.*, 2021). The user-friendly nature of Grasshopper allows architects, designers and others without proficiency in programming to use this methodology. Undoubtedly, the use of open-source plugins in Grasshopper has increased its popularity in research, but also spurred the integration of Grasshopper and its environmental plugins into educational curriculums, and it is fast becoming an indispensable tool in

practice. The UTCI results reported in this study are in degrees Celsius, which describe how pedestrians "feel" within a street canyon, and hence, designers can use these results as they are, without the need for further interpretation. The Egyptian government's current initiative to amend the design regulations is not yet fully implemented. Such amendments can be extended to include climate informed design guidelines such as those reported in this study. Moreover, this paper's methodology can be applied to district and small urban scale studies (Ibrahim *et al.*, 2021), giving the opportunity to include performance driven insights into the design guidelines at different scales, thereby promoting the creation of resilient and sustainable built environments which ensure pedestrians' health and well-being.

5 Study limitations

The simulation workflow presented in this study is based on an aggregated bottom-up approach by chaining the inputs and outputs of validated software engines, i.e., EnergyPlus and UWG, within the Grasshopper environment. This approach is appropriate in parametric studies aiming to support urban planners and designers in the planning stage, where the use of standardised design parameters facilitates the simulation of a higher number of case studies, whose results are most needed in this stage. The applicability of the workflow is, however, confronted by the necessity to balance the computational cost of including detailed bottom-up approaches, e.g. running CFD analyses, and the reliability of the model's performance. In this study, we chose not to include wind analyses in favour of running a remarkably increased number of geometric permutations, since the workflow has shown considerable reliability using wind speeds from the IWEC file. Other approaches available in Grasshopper include wind analyses using Butterfly (Mackey *et al.*, 2017) or Eddy3D (Natanian *et al.*, 2020) which produce wind factors, the ratio between the simulated wind speeds and the inlet wind speed generated from a number of directions. These approaches, however, are not as accurate as if the turbulent heat exchanges are considered within the model, which is a feature in the OpenFOAM software, but is not yet integrated (currently under development) in either of the two plug-ins.

Furthermore, compared with field measurements, it was shown that the ladybug-tools model underestimates the UTCI by some 3.5 °C. As mentioned in section 2.2, the main deviation stems from the differences between the simulation model and the real case in three main parameters. Firstly, in

sunlit hours, the radiation model mainly depends on the global horizontal radiation, retrieved from the weather file, which might suggest inaccuracies if not identical to reality. Secondly, the definition of the ground surface as the upper surface of an EnergyPlus thermal zone, assuming all other surfaces are adiabatic. Currently, there is no evidence from the literature about the convective nor the long-wave radiative heat transfer with this ground zone (Evola *et al.*, 2020). Finally, the spatial resolution of the simulation model which may suggest inaccuracies regarding the sun obstruction angles. Notwithstanding, these differences are consistent over the hypothetical cases, and hence can be accepted for the purpose of running a comparative analysis in this pre-design stage. Further improvements to the model need to be made in detailed analyses.

For most geometry configurations, this study has recommended using high aspect ratios for improved thermal comfort conditions. These configurations, nonetheless, might not seem applicable in practice in Egypt, although they are extensively found in other countries with similar climates, for instance Morocco (Johansson, 2006) (Figure 16-left) and Algeria (Bourbia *et al.*, 2010). The fact that Egypt has suffered from urban sprawl since 1950 with around 50% of the existing building stock not complying with the building regulations (Edeisy *et al.*, 2018) has spurred the government to instigate a redevelopment campaign for slums. Figure 16-right shows a sprawled area in Cairo, included in the government redevelopment action plan, where the rightmost part of the image is a neighbourhood, newly constructed in compliance with the Construction Act. That is to say, the limitation of applying these configurations in Egypt is subject to the interventions by stakeholders and decision makers in the design policies and regulations.

Figure 16: Satellite images of a neighbourhood in Fez, Morocco (Left), and Ezbet El-Haggana, Cairo, Egypt (right). The rightmost part of the image is a public sector newly constructed neighbourhood.

6 Conclusion

This study investigated the effect of H/W ratio and orientation of urban canyons on the outdoor thermal comfort represented by the UTCI. The Ladybug-tools microclimate model has shown its capability to capture the dynamic patterns of solar radiation and the resultant outdoor thermal comfort. In a hot arid climate, it was shown that modification of H/W and orientation can reduce the UTCI by almost 6 °C. Higher H/W ratios are favourable in N-S, NE-SW and NW-SE canyons and have the potential to reduce the heat stress in the urban canyon, whereas the more canyons are orientated E-W, the less effect H/W ratios have on the microclimate. Moreover, asymmetrical urban canyons are a feasible option, so long as taller buildings cast shadows on the canyon ground and shorter buildings, allowing for openness to the sky for convective cooling. The obtained UTCI thermal stress could be reduced significantly if the calculations were made on a typical day rather than an extreme one, not to mention the uncertainties of the weather file (Chinazzo *et al.*, 2015). Given the shorter time required for computer simulations, which exceeds a thousand runs per day, this study could be applied in various climatic contexts. In Egypt, where the summer solar shading is prioritised over the winter solar heat gain, the study focused on the compromise between different H/W's and orientations in summer. In other climatic zones, seasonal variations should be considered. The study provides climate-based insights for urban planners aiming at creating healthy and sustainable built environments.

Data Availability Statement

Data available in a publicly accessible repository. The data presented in this study are openly available in University of Bath Research Data Archive at [https://doi.org/10.15125/BATH-01045] (Ibrahim, 2021).

References

Ahmed, K. (1994). *A comparative analysis of the outdoor thermal environment of the urban vernacular and the contemporary development: case studies in Dhaka.* Paper presented at the Proceedings of the 11 th PLEA International Conference, Dead Sea.

Ali-Toudert, F. (2005). *Dependence of Outdoor Thermal Comfort on Street Design in Hot and Dry Climate.* (PhD). Institutes der Universität Freiburg, Freiburg, Germany. (15)

Ali-Toudert, F., Djenane, M., Bensalem, R., & Mayer, H. (2005). Outdoor thermal comfort in the old desert city of Beni-Isguen, Algeria. *Climate Research, 28*(3), 243-256. doi:http://doi.org/10.3354/cr028243

Ali-Toudert, F., & Mayer, H. (2006). Numerical study on the effects of aspect ratio and orientation of an urban street canyon on outdoor thermal comfort in hot and dry climate. *Building and Environment, 41*(2), 94-108. doi:http:\\doi.org\10.1016/j.buildenv.2005.01.013

Ali-Toudert, F., & Mayer, H. (2007). Effects of asymmetry, galleries, overhanging fac¸ades and vegetation on thermal comfort in urban street canyons. *Solar Energy, 81*(6), 742–754. doi:https://doi.org/10.1016/j.solener.2006.10.007

Ampatzidis, P., & Kershaw, T. (2020). A review of the impact of blue space on the urban microclimate. *Science of the total environment, 730*, 1-18. doi:https://doi.org/10.1016/j.scitotenv.2020.139068

Andreou, E. (2013). Thermal comfort in outdoor spaces and urban canyon microclimate. *Renewable energy, 55*, 182-188. doi:http://dx.doi.org/10.1016/j.renene.2012.12.040

Arens, E., Hoyt, T., Zhou, X., Huang, L., Zhang, H., & Schiavon, S. (2015). Modeling the comfort effects of short-wave solar radiation indoors. *Building and Environment, 88*, 3-9. doi:http://dx.doi.org/10.1016/j.buildenv.2014.09.004

ASHRAE. ANSI/ASHRAE Standard 55-2017: Thermal environmental conditions for human occupancy. In (pp. 22-29): American Society of Heating, Refrigerating and Air-Conditioning Engineers, Atlanta, GA, USA, 2017.

Blazejczyk, K. (2005). *MENEX_2005. The Updated Version of Man-Environment Heat Exchange Model*.

Blazejczyk, K., Epstein, Y., Jendritzky, G., Staiger, H., & Tinz, B. (2012). Comparison of UTCI to selected thermal indices. *International journal of biometeorology, 56*(3), 515-535. doi:https://doi.org/10.1007/s00484-011-0453-2

Bourbia, F., & Boucheriba, F. (2010). Impact of street design on urban microclimate for semi arid climate (Constantine). *Renewable energy, 35*(2), 343-347. doi:https://doi.org/10.1016/j.renene.2009.07.017

British Standards Institution, BSI. (2001). Ergonomics of the thermal environment—Instruments for measuring physical quantities (BS EN ISO 7726:2001). In (pp. 51).

Bröde, P., Fiala, D., Błażejczyk, K., Holmér, I., Jendritzky, G., Kampmann, B., Tinz, B., & Havenith, G. (2012). Deriving the operational procedure for the Universal Thermal Climate Index (UTCI). *International journal of biometeorology, 56*(3), 481-494. doi:https://doi.org/10.1007/s00484-011-0454-1

Bueno, B., Norford, L., Hidalgo, J., & Pigeon, G. (2013). The urban weather generator. *Journal of Building Performance Simulation, 6*(4), 269-281. doi:https://doi.org/10.1080/19401493.2012.718797

Bueno, B., Roth, M., Norford, L., & Li, R. (2014). Computationally efficient prediction of canopy level urban air temperature at the neighbourhood scale. *Urban Climate, 9*, 35-53. doi:http://dx.doi.org/10.1016/j.uclim.2014.05.005

CAPMAS. (2019). *Bulletin of Housing in Egypt*. (71-21123-2019). Cairo, Egypt: Central Agency for Public Mobilization & Statistics Retrieved from https://www.capmas.gov.eg/Pages/Publications.aspx?page_id=5104&Year=23415

Chinazzo, G., Rastogi, P., & Andersen, M. (2015). Assessing robustness regarding weather uncertainties for energy-efficiency-driven building refurbishments. *Energy Procedia, 78*, 931-936. doi:doi: 10.1016/j.egypro.2015.11.021

Coccolo, S., Kämpf, J., Scartezzini, J.-L., & Pearlmutter, D. (2016). Outdoor human comfort and thermal stress: A comprehensive review on models and standards. *Urban Climate, 18*, 33-57. doi:http://dx.doi.org/10.1016/j.uclim.2016.08.004

Crawley, D. B., Lawrie, L. K., Winkelmann, F. C., Buhl, W. F., Huang, Y. J., Pedersen, C. O., Strand, R. K., Liesen, R. J., Fisher, D. E., & Witte, M. J. (2001). EnergyPlus: creating a new-generation building energy simulation program. *Energy and Buildings, 33*(4), 319-331. doi:https://doi.org/10.1016/S0378-7788(00)00114-6

DoE. (2020). Weather Data. Retrieved from https://energyplus.net/weather

Edeisy, M., & Cecere, C. (2018). Energy Efficiency for Egyptian Housing: Code Compliance and Enforcement. *International Journal of the Constructed Environment, 9*(3), 1-19. doi:http://doi.org/10.18848/2154-8587/CGP/v09i03/1-15

Emmanuel, R., Rosenlund, H., & Johansson, E. (2007). Urban shading—a design option for the tropics? A study in Colombo, Sri Lanka. *International Journal of Climatology: A Journal of the Royal Meteorological Society, 27*(14), 1995-2004. doi:10.1002/joc.1609

Engineering-ToolBox. (2001). Engineering ToolBox. Retrieved from https://www.engineeringtoolbox.com/

Evola, G., Costanzo, V., Magrì, C., Margani, G., Marletta, L., & Naboni, E. (2020). A novel comprehensive workflow for modelling outdoor thermal comfort and energy demand in urban canyons: results and critical issues. *Energy and Buildings, 216*(109946), 1-19. doi:https://doi.org/10.1016/j.enbuild.2020.109946

Extech. (2021). Extech HT30: Heat Stress WBGT (Wet Bulb Globe Temperature) Meter. Retrieved from http://www.extech.com/ht30/

Fahmy, M. (2010). *Interactive urban form design of local climate scale in hot semi-arid zone.* (PhD). The University of Sheffield,

Fahmy, M., Ibrahim, Y., Hanafi, E., & Barakat, M. (2018). Would LEED-UHI greenery and high albedo strategies mitigate climate change at neighborhood scale in Cairo, Egypt? *Building Simulation, 11*(6), 1273-1288.

Fanger, P. O. (1972). *Thermal comfort; Analysis and applications in environmental engineering*. NewYork: McGraw-Hill, first published in 1970, Danish Technical Press, Copenhagen.

Fiala, D., Havenith, G., Bröde, P., Kampmann, B., & Jendritzky, G. (2012). UTCI-Fiala multi-node model of human heat transfer and temperature regulation. *International journal of biometeorology, 56*(3), 429-441. doi:https://doi.org/10.1007/s00484-011-0424-7

Futcher, J. A., Kershaw, T., & Mills, G. (2013). Urban form and function as building performance parameters. *Building and Environment, 62*, 112-123. doi:https://doi.org/10.1016/j.buildenv.2013.01.021

Galal, O. M., Sailor, D. J., & Mahmoud, H. (2020). The impact of urban form on outdoor thermal comfort in hot arid environments during daylight hours, case study: New Aswan. *Building and Environment, 184*(107222), 1-15. doi:https://doi.org/10.1016/j.buildenv.2020.107222

Giannopoulou, K., Santamouris, M., Livada, I., Georgakis, C., & Caouris, Y. (2010). The impact of canyon geometry on intra urban and urban: suburban night temperature differences under warm weather conditions. *Pure and applied geophysics, 167*(11), 1433-1449. doi:https://doi.org/10.1007/s00024-010-0099-8

Golany, G. S. (1996). Urban design morphology and thermal performance. *Atmospheric Environment, 30*(3), 455-465. doi:https://doi.org/10.1016/1352-2310(95)00266-9

Grimmond, C., Roth, M., Oke, T. R., Au, Y., Best, M., Betts, R., Carmichael, G., Cleugh, H., Dabberdt, W., & Emmanuel, R. (2010). Climate and more sustainable cities: climate information for

improved planning and management of cities (producers/capabilities perspective). *Procedia Environmental Sciences, 1*, 247-274. doi:https://doi.org/10.1016/j.proenv.2010.09.016

Havenith, G., Fiala, D., Błazejczyk, K., Richards, M., Bröde, P., Holmér, I., Rintamaki, H., Benshabat, Y., & Jendritzky, G. (2012). The UTCI-clothing model. *International journal of biometeorology, 56*(3), 461-470. doi:https://doi.org/10.1007/s00484-011-0451-4

He, B.-J., Ding, L., & Prasad, D. (2019). Enhancing urban ventilation performance through the development of precinct ventilation zones: A case study based on the Greater Sydney, Australia. *Sustainable Cities and Society, 47*(101472), 14. doi:https://doi.org/10.1016/j.scs.2019.101472

Höppe, P. (1999). The physiological equivalent temperature–a universal index for the biometeorological assessment of the thermal environment. *International journal of biometeorology, 43*(2), 71-75. doi:https://doi.org/10.1007/s004840050118

[dataset] Ibrahim, Y. (2021). *Dataset for "A parametric optimisation study of urban geometry design to assess outdoor thermal comfort"*. Retrieved from: https://researchdata.bath.ac.uk/1045. Bath: University of Bath Research Data Archive. doi:https://doi.org/10.15125/BATH-01045

Ibrahim, Y., Kershaw, T., & Shepherd, P. (2020a). *Improvement of the Ladybug-tools microclimate workflow: A verification study*. Paper presented at the Building Simulation and Optimization 2020, Loughborough University, Loughborough, UK.

Ibrahim, Y., Kershaw, T., & Shepherd, P. (2020b). *A methodology For Modelling Microclimate: A Ladybug-tools and ENVI-met Verification Study*. Paper presented at the 35th PLEA Conference. Sustainable Architecture and Urban Design: Planning Post Carbon Cities, A Coruña, Spain, 1–3 September.

Ibrahim, Y., Kershaw, T., Shepherd, P., & Coley, D. (2021). On the Optimisation of Urban form Design, Energy Consumption and Outdoor Thermal Comfort Using a Parametric Workflow in a Hot Arid Zone. *Energies, 14*(4026), 22. doi:https:// doi.org/10.3390/en14134026

Jamei, E., & Rajagopalan, P. (2019). Effect of street design on pedestrian thermal comfort. *Architectural Science Review, 62*(2), 92-111. doi:https://doi.org/10.1080/00038628.2018.1537236

Jamei, E., Rajagopalan, P., Seyedmahmoudian, M., & Jamei, Y. (2016). Review on the impact of urban geometry and pedestrian level greening on outdoor thermal comfort. *Renewable and Sustainable Energy Reviews, 54*, 1002-1017. doi:http://dx.doi.org/10.1016/j.rser.2015.10.104

Johansson, E. (2006). Influence of urban geometry on outdoor thermal comfort in a hot dry climate: A study in Fez, Morocco. *Building and Environment, 41*(10), 1326-1338. doi:https://doi.org/10.1016/j.buildenv.2005.05.022

Kovats, R. S., & Hajat, S. (2008). Heat stress and public health: a critical review. *Annu. Rev. Public Health, 29*, 41-55. doi:10.1146/annurev.publhealth.29.020907.090843

Krüger, E., Pearlmutter, D., & Rasia, F. (2010). Evaluating the impact of canyon geometry and orientation on cooling loads in a high-mass building in a hot dry environment. *Applied Energy, 87*(6), 2068-2078.

Labib, R., & Beltran, L. (2015). *Optimized Street Design to Balance Outdoor Thermal Comfort And Indoor Daylighting Performance Within Large Scale Urban Settings in Hot Arid Climates*.

Lin, P., Gou, Z., Lau, S. S.-Y., & Qin, H. (2017). The impact of urban design descriptors on outdoor thermal environment: A literature review. *Energies, 10*(12), 2151. doi:doi:10.3390/en10122151

Mackey, C., Galanos, T., Norford, L., Roudsari, M. S., & Architects, P. (2017). *Wind, sun, surface temperature, and heat island: critical variables for high-resolution outdoor thermal comfort.* Paper presented at the Proceedings of the 15th International conference of Building Performance Simulation Association. San Francisco, USA.

Mahdy, M. M. (2014). *Applying architecture simulation tools to assess building sustainable design: Adapting the Egyptian residential energy code for climate change.* (PhD). University of Kent, Retrieved from https://books.google.co.uk/books?id=2mDjvgEACAAJ

Ministry of Housing Utilities & Urban Communities, MHUUC. (2008). The Executive Regulations for the Egyptian Unified Construction Act. In (pp. 163). Cairo, Egypt: General Organisation for Physical Planning.

Naboni, E., Meloni, M., Coccolo, S., Kaempf, J., & Scartezzini, J.-L. (2017). An overview of simulation tools for predicting the mean radiant temperature in an outdoor space. *Energy Procedia, 122*, 1111-1116.

Naboni, E., Meloni, M., Mackey, C., & Kaempf, J. (2019a). *The simulation of mean radiant temperature in outdoor conditions: A review of software tools capabilities*. Paper presented at the Proceedings of the 16th IBPSA Conference, Rome, Italy, Sept. 2-4, 2019.

Naboni, E., Ofria, L., & Danzo, E. (2019b). *A Parametric Workflow to Conceive Facades as Indoor and Outdoor Climate Givers*. Paper presented at the SimAUD 2019, April 07-09: Atlanta, Georgia.

Natanian, J., Kastner, P., Dogan, T., & Auer, T. (2020). From energy performative to livable Mediterranean cities: An annual outdoor thermal comfort and energy balance cross-climatic typological study. *Energy and Buildings, 224*(110283). doi:https://doi.org/10.1016/j.enbuild.2020.110283

Niachou, K., Hassid, S., Santamouris, M., & Livada, I. (2008). Experimental performance investigation of natural, mechanical and hybrid ventilation in urban environment. *Building and Environment, 43*(8), 1373-1382. doi:https://doi.org/10.1016/j.buildenv.2007.01.046

Oke, T. (1995). The heat island of the urban boundary layer: characteristics, causes and effects. In *Wind climate in cities* (pp. 81-107). Berlin/Heidelberg, Germany: Springer.

Oke, T., Mills, G., Christen, A., & Voogt, J. (2017). *Urban Climates*. Cambridge Cambridge University Press.

Oke, T. R. (1988). Street Design and Urban Canopy Layer Climate. *Energy and Buildings, 11*(1-3), 103-113. doi:https://doi.org/10.1016/0378-7788(88)90026-6

Onset. (2021). HOBO U30 Data Loggers. Retrieved from http://www.onsetcomp.com/products/data-loggers/U30-data-loggers

Pearlmutter, D., Berliner, P., & Shaviv, E. (2007). Urban climatology in arid regions: current research in the Negev desert. *International Journal of Climatology, 27*(14), 1875-1885. doi:https://doi.org/10.1002/joc.1523

Perini, K., & Magliocco, A. (2014). Effects of vegetation, urban density, building height, and atmospheric conditions on local temperatures and thermal comfort. *Urban Forestry & Urban Greening, 13*(3), 495-506. doi:http://dx.doi.org/10.1016/j.ufug.2014.03.003

Potchter, O., Cohen, P., Lin, T.-P., & Matzarakis, A. (2018). Outdoor human thermal perception in various climates: A comprehensive review of approaches, methods and quantification. *Science of the total environment, 631*, 390-406. doi:https://doi.org/10.1016/j.scitotenv.2018.02.276

Qaid, A., & Ossen, D. R. (2015). Effect of asymmetrical street aspect ratios on microclimates in hot, humid regions. *International journal of biometeorology, 59*(6), 657-677. doi:https://doi.org/10.1007/s00484-014-0878-5

Ratti, C., Raydan, D., & Steemers, K. (2003). Building form and environmental performance: archetypes, analysis and an arid climate. *Energy and Buildings, 35*(1), 49-59. doi:https://doi.org/10.1016/S0378-7788(02)00079-8

Roudsari, M. S., & Mackey, C. (2020). Ladybug-tools. Retrieved from https://www.ladybug.tools/

Ruefenacht, L., Sukma, A., Acero, J. A., & Nevat, I. (2020). *Climate-responsive design guidelines: Urban design guidelines to improve outdoor thermal comfort in the southern shore area of singapore*. Retrieved from

Shalaby, A. S., & Shafey, A. M. (2018). Optimizing the Thermal Performance of Street Canyons in New Cairo, Egypt, Using ENVI-met. *5*(4), 5639-5654.

Sharmin, T., Steemers, K., & Matzarakis, A. (2017). Microclimatic modelling in assessing the impact of urban geometry on urban thermal environment. *Sustainable Cities and Society, 34*, 293-308. doi:http://dx.doi.org/10.1016/j.scs.2017.07.006

Sini, J.-F., Anquetin, S., & Mestayer, P. G. (1996). Pollutant dispersion and thermal effects in urban street canyons. *Atmospheric Environment, 30*(15), 2659-2677. doi:https://doi.org/10.1016/1352-2310(95)00321-5

Stewart, I. D., & Oke, T. R. (2012). Local climate zones for urban temperature studies. *Bulletin of the American Meteorological Society, 93*(12), 1879-1900. doi:https://doi.org/10.1175/BAMS-D-11-00019.1

Tomasetti, T. (2020). Core Studio. Retrieved from http://core.thorntontomasetti.com/

Toparlar, Y., Blocken, B., Vos, P. v., Van Heijst, G., Janssen, W., van Hooff, T., Montazeri, H., & Timmermans, H. (2015). CFD simulation and validation of urban microclimate: A case study for Bergpolder Zuid, Rotterdam. *Building and Environment, 83*, 79-90. doi:http://dx.doi.org/10.1016/j.buildenv.2014.08.004

United Nations, Department of Economic and Social Affairs Population Division. (2018). *World Urbanization Prospects: The 2018 Revision*. Retrieved from New York: United Nations: https://population.un.org/wup/Publications/Files/WUP2018-Report.pdf

Wagdy, A., Sherif, A., Sabry, H., Arafa, R., & Mashaly, I. (2017). Daylighting simulation for the configuration of external sun-breakers on south oriented windows of hospital patient rooms under a clear desert sky. *Solar Energy, 149*, 164-175. doi:http://dx.doi.org/10.1016/j.solener.2017.04.009

Watkins, R., Palmer, J., & Kolokotroni, M. (2007). Increased temperature and intensification of the urban heat island: implications for human comfort and urban design. *Built Environment, 33*(1), 85-96.

Witte, M. J., Henninger, R. H., Glazer, J., & Crawley, D. B. *Testing and validation of a new building energy simulation program*. Paper presented at the 7th IBSPA Conference.